Angular correlations in three-jet events in ep collisions at HERA

H. Abramowicz *et al.* (ZEUS Collaboration)

Phys. Rev. D **85**, 052008 — Published 27 March 2012

DOI: 10.1103/PhysRevD.85.052008

Angular correlations in three-jet events in ep collisions at HERA

ZEUS Collaboration

Abstract

Three-jet production in deep inelastic ep scattering and photoproduction was investigated with the ZEUS detector at HERA using an integrated luminosity of up to 127 pb^{-1}. Measurements of differential cross sections are presented as functions of angular correlations between the three jets in the final state and the proton-beam direction. These correlations provide a stringent test of perturbative QCD and show sensitivity to the contributions from different colour configurations. Fixed-order perturbative calculations assuming the values of the colour factors C_F, C_A and T_F as derived from a variety of gauge groups were compared to the measurements to study the underlying gauge group symmetry. The measured angular correlations in the deep inelastic ep scattering and photoproduction regimes are consistent with the admixture of colour configurations as predicted by SU(3) and disfavour other symmetry groups, such as SU(N) in the limit of large N.

The ZEUS Collaboration

H. Abramowicz[45,ah], I. Abt[35], L. Adamczyk[13], M. Adamus[54], R. Aggarwal[7,c], S. Antonelli[4], P. Antonioli[3], A. Antonov[33], M. Arneodo[50], V. Aushev[26,27,z], Y. Aushev,[27,z,aa], O. Bachynska[15], A. Bamberger[19], A.N. Barakbaev[25], G. Barbagli[17], G. Bari[3], F. Barreiro[30], N. Bartosik[27,ab], D. Bartsch[5], M. Basile[4], O. Behnke[15], J. Behr[15], U. Behrens[15], L. Bellagamba[3], A. Bertolin[39], S. Bhadra[57], M. Bindi[4], C. Blohm[15], V. Bokhonov[26,z], T. Bołd[13], K. Bondarenko[27], E.G. Boos[25], K. Borras[15], D. Boscherini[3], D. Bot[15], I. Brock[5], E. Brownson[56], R. Brugnera[40], N. Brümmer[37], A. Bruni[3], G. Bruni[3], B. Brzozowska[53], P.J. Bussey[20], B. Bylsma[37], A. Caldwell[35], M. Capua[8], R. Carlin[40], C.D. Catterall[57], S. Chekanov[1], J. Chwastowski[12,e], J. Ciborowski[53,al], R. Ciesielski[15,g], L. Cifarelli[4], F. Cindolo[3], A. Contin[4], A.M. Cooper-Sarkar[38], N. Coppola[15,h], M. Corradi[3], F. Corriveau[31], M. Costa[49], G. D'Agostini[43], F. Dal Corso[39], J. del Peso[30], R.K. Dementiev[34], S. De Pasquale[4,a], M. Derrick[1], R.C.E. Devenish[38], D. Dobur[19,s], B.A. Dolgoshein [33,†], G. Dolinska[26,27], A.T. Doyle[20], V. Drugakov[16], L.S. Durkin[37], S. Dusini[39], Y. Eisenberg[55], P.F. Ermolov [34,†], A. Eskreys [12,†], S. Fang[15,i], S. Fazio[8], J. Ferrando[38], M.I. Ferrero[49], J. Figiel[12], M. Forrest[20,v], B. Foster[38,ad], G. Gach[13], A. Galas[12], E. Gallo[17], A. Garfagnini[40], A. Geiser[15], I. Gialas[21,w], L.K. Gladilin[34,ac], D. Gladkov[33], C. Glasman[30], O. Gogota[26,27], Yu.A. Golubkov[34], P. Göttlicher[15,j], I. Grabowska-Bołd[13], J. Grebenyuk[15], I. Gregor[15], G. Grigorescu[36], G. Grzelak[53], O. Gueta[45], M. Guzik[13], C. Gwenlan[38,ae], T. Haas[15], W. Hain[15], R. Hamatsu[48], J.C. Hart[44], H. Hartmann[5], G. Hartner[57], E. Hilger[5], D. Hochman[55], R. Hori[47], K. Horton[38,af], A. Hüttmann[15], Z.A. Ibrahim[10], Y. Iga[42], R. Ingbir[45], M. Ishitsuka[46], H.-P. Jakob[5], F. Januschek[15], M. Jimenez[30], T.W. Jones[52], M. Jüngst[5], I. Kadenko[27], B. Kahle[15], S. Kananov[45], T. Kanno[46], U. Karshon[55], F. Karstens[19,t], I.I. Katkov[15,k], M. Kaur[7], P. Kaur[7,c], A. Keramidas[36], L.A. Khein[34], J.Y. Kim[9], D. Kisielewska[13], S. Kitamura[48,aj], R. Klanner[22], U. Klein[15,l], E. Koffeman[36], P. Kooijman[36], Ie. Korol[26,27], I.A. Korzhavina[34,ac], A. Kotański[14,f], U. Kötz[15], H. Kowalski[15], O. Kuprash[15], M. Kuze[46], A. Lee[37], B.B. Levchenko[34], A. Levy[45], V. Libov[15], S. Limentani[40], T.Y. Ling[37], M. Lisovyi[15], E. Lobodzinska[15], W. Lohmann[16], B. Löhr[15], E. Lohrmann[22], K.R. Long[23], A. Longhin[39], D. Lontkovskyi[15], O.Yu. Lukina[34], J. Maeda[46,ai], S. Magill[1], I. Makarenko[15], J. Malka[15], R. Mankel[15], A. Margotti[3], G. Marini[43], J.F. Martin[51], A. Mastroberardino[8], M.C.K. Mattingly[2], I.-A. Melzer-Pellmann[15], S. Mergelmeyer[5], S. Miglioranzi[15,m], F. Mohamad Idris[10], V. Monaco[49], A. Montanari[15], J.D. Morris[6,b], K. Mujkic[15,n], B. Musgrave[1], K. Nagano[24], T. Namsoo[15,o], R. Nania[3], A. Nigro[43], Y. Ning[11], T. Nobe[46], U. Noor[57], D. Notz[15], R.J. Nowak[53], A.E. Nuncio-Quiroz[5], B.Y. Oh[41], N. Okazaki[47], K. Oliver[38], K. Olkiewicz[12], Yu. Onishchuk[27], K. Papageorgiu[21], A. Parenti[15], E. Paul[5], J.M. Pawlak[53], B. Pawlik[12], P. G. Pelfer[18], A. Pellegrino[36], W. Perlański[53,am], H. Perrey[15], K. Piotrzkowski[29], P. Pluciński[54,an], N.S. Pokrovskiy[25], A. Polini[3], A.S. Proskuryakov[34], M. Przybycień[13], A. Raval[15], D.D. Reeder[56], B. Reisert[35], Z. Ren[11], J. Repond[1], Y.D. Ri[48,ak], A. Robertson[38], P. Roloff[15,m], I. Rubinsky[15], M. Ruspa[50], R. Sacchi[49], A. Salii[27], U. Samson[5], G. Sartorelli[4], A.A. Savin[56], D.H. Saxon[20], M. Schioppa[8], S. Schlenstedt[16], P. Schleper[22], W.B. Schmidke[35], U. Schneekloth[15], V. Schönberg[5], T. Schörner-Sadenius[15], J. Schwartz[31], F. Sciulli[11], L.M. Shcheglova[34], R. Shehzadi[5], S. Shimizu[47,m], I. Singh[7,c], I.O. Skillicorn[20], W. Słomiński[14], W.H. Smith[56], V. Sola[49], A. Solano[49], D. Son[28], V. Sosnovtsev[33], A. Spiridonov[15,p], H. Stadie[22], L. Stanco[39], A. Stern[45], T.P. Stewart[51], A. Stifutkin[33], P. Stopa[12], S. Suchkov[33], G. Susinno[8], L. Suszycki[13],

J. Sztuk-Dambietz[22], D. Szuba[22], J. Szuba[15,q], A.D. Tapper[23], E. Tassi[8,d], J. Terrón[30], T. Theedt[15], H. Tiecke[36], K. Tokushuku[24,x], O. Tomalak[27], J. Tomaszewska[15,r], T. Tsurugai[32], M. Turcato[22], T. Tymieniecka[54,ao], M. Vázquez[36,m], A. Verbytskyi[15], O. Viazlo[26,27], N.N. Vlasov[19,u], O. Volynets[27], R. Walczak[38], W.A.T. Wan Abdullah[10], J.J. Whitmore[41,ag], L. Wiggers[36], M. Wing[52], M. Wlasenko[5], G. Wolf[15], H. Wolfe[56], K. Wrona[15], A.G. Yagües-Molina[15], S. Yamada[24], Y. Yamazaki[24,y], R. Yoshida[1], C. Youngman[15], A.F. Żarnecki[53], L. Zawiejski[12], O. Zenaiev[15], W. Zeuner[15,m], B.O. Zhautykov[25], N. Zhmak[26,z], C. Zhou[31], A. Zichichi[4], Z. Zolkapli[10], M. Zolko[27], D.S. Zotkin[34]

[1] *Argonne National Laboratory, Argonne, Illinois 60439-4815, USA* [A]
[2] *Andrews University, Berrien Springs, Michigan 49104-0380, USA*
[3] *INFN Bologna, Bologna, Italy* [B]
[4] *University and INFN Bologna, Bologna, Italy* [B]
[5] *Physikalisches Institut der Universität Bonn, Bonn, Germany* [C]
[6] *H.H. Wills Physics Laboratory, University of Bristol, Bristol, United Kingdom* [D]
[7] *Panjab University, Department of Physics, Chandigarh, India*
[8] *Calabria University, Physics Department and INFN, Cosenza, Italy* [B]
[9] *Institute for Universe and Elementary Particles, Chonnam National University, Kwangju, South Korea*
[10] *Jabatan Fizik, Universiti Malaya, 50603 Kuala Lumpur, Malaysia* [E]
[11] *Nevis Laboratories, Columbia University, Irvington on Hudson, New York 10027, USA* [F]
[12] *The Henryk Niewodniczanski Institute of Nuclear Physics, Polish Academy of Sciences, Krakow, Poland* [G]
[13] *AGH-University of Science and Technology, Faculty of Physics and Applied Computer Science, Krakow, Poland* [H]
[14] *Department of Physics, Jagellonian University, Cracow, Poland*
[15] *Deutsches Elektronen-Synchrotron DESY, Hamburg, Germany*
[16] *Deutsches Elektronen-Synchrotron DESY, Zeuthen, Germany*
[17] *INFN Florence, Florence, Italy* [B]
[18] *University and INFN Florence, Florence, Italy* [B]
[19] *Fakultät für Physik der Universität Freiburg i.Br., Freiburg i.Br., Germany*
[20] *School of Physics and Astronomy, University of Glasgow, Glasgow, United Kingdom* [D]
[21] *Department of Engineering in Management and Finance, Univ. of the Aegean, Chios, Greece*
[22] *Hamburg University, Institute of Experimental Physics, Hamburg, Germany* [I]
[23] *Imperial College London, High Energy Nuclear Physics Group, London, United Kingdom* [D]
[24] *Institute of Particle and Nuclear Studies, KEK, Tsukuba, Japan* [J]
[25] *Institute of Physics and Technology of Ministry of Education and Science of Kazakhstan, Almaty, Kazakhstan*
[26] *Institute for Nuclear Research, National Academy of Sciences, Kyiv, Ukraine*
[27] *Department of Nuclear Physics, National Taras Shevchenko University of Kyiv, Kyiv, Ukraine*
[28] *Kyungpook National University, Center for High Energy Physics, Daegu, South Korea* [K]
[29] *Institut de Physique Nucléaire, Université Catholique de Louvain, Louvain-la-Neuve, Belgium* [L]
[30] *Departamento de Física Teórica, Universidad Autónoma de Madrid, Madrid, Spain* [M]
[31] *Department of Physics, McGill University, Montréal, Québec, Canada H3A 2T8* [N]
[32] *Meiji Gakuin University, Faculty of General Education, Yokohama, Japan* [J]

[33] *Moscow Engineering Physics Institute, Moscow, Russia* [O]
[34] *Moscow State University, Institute of Nuclear Physics, Moscow, Russia* [P]
[35] *Max-Planck-Institut für Physik, München, Germany*
[36] *NIKHEF and University of Amsterdam, Amsterdam, Netherlands* [Q]
[37] *Physics Department, Ohio State University, Columbus, Ohio 43210, USA* [A]
[38] *Department of Physics, University of Oxford, Oxford, United Kingdom* [D]
[39] *INFN Padova, Padova, Italy* [B]
[40] *Dipartimento di Fisica dell' Università and INFN, Padova, Italy* [B]
[41] *Department of Physics, Pennsylvania State University, University Park, Pennsylvania 16802, USA* [F]
[42] *Polytechnic University, Sagamihara, Japan* [J]
[43] *Dipartimento di Fisica, Università 'La Sapienza' and INFN, Rome, Italy* [B]
[44] *Rutherford Appleton Laboratory, Chilton, Didcot, Oxon, United Kingdom* [D]
[45] *Raymond and Beverly Sackler Faculty of Exact Sciences, School of Physics, Tel Aviv University, Tel Aviv, Israel* [R]
[46] *Department of Physics, Tokyo Institute of Technology, Tokyo, Japan* [J]
[47] *Department of Physics, University of Tokyo, Tokyo, Japan* [J]
[48] *Tokyo Metropolitan University, Department of Physics, Tokyo, Japan* [J]
[49] *Università di Torino and INFN, Torino, Italy* [B]
[50] *Università del Piemonte Orientale, Novara, and INFN, Torino, Italy* [B]
[51] *Department of Physics, University of Toronto, Toronto, Ontario, Canada M5S 1A7* [N]
[52] *Physics and Astronomy Department, University College London, London, United Kingdom* [D]
[53] *Faculty of Physics, University of Warsaw, Warsaw, Poland*
[54] *National Centre for Nuclear Research, Warsaw, Poland*
[55] *Department of Particle Physics and Astrophysics, Weizmann Institute, Rehovot, Israel*
[56] *Department of Physics, University of Wisconsin, Madison, Wisconsin 53706, USA* [A]
[57] *Department of Physics, York University, Ontario, Canada M3J 1P3* [N]

[A] supported by the US Department of Energy
[B] supported by the Italian National Institute for Nuclear Physics (INFN)
[C] supported by the German Federal Ministry for Education and Research (BMBF), under contract No. 05 H09PDF
[D] supported by the Science and Technology Facilities Council, UK
[E] supported by an FRGS grant from the Malaysian government
[F] supported by the US National Science Foundation. Any opinion, findings and conclusions or recommendations expressed in this material are those of the authors and do not necessarily reflect the views of the National Science Foundation.
[G] supported by the Polish Ministry of Science and Higher Education as a scientific project No. DPN/N188/DESY/2009
[H] supported by the Polish Ministry of Science and Higher Education and its grants for Scientific Research
[I] supported by the German Federal Ministry for Education and Research (BMBF), under contract No. 05h09GUF, and the SFB 676 of the Deutsche Forschungsgemeinschaft (DFG)
[J] supported by the Japanese Ministry of Education, Culture, Sports, Science and Technology (MEXT) and its grants for Scientific Research
[K] supported by the Korean Ministry of Education and Korea Science and Engineering Foundation
[L] supported by FNRS and its associated funds (IISN and FRIA) and by an Inter-University Attraction Poles Programme subsidised by the Belgian Federal Science Policy Office
[M] supported by the Spanish Ministry of Education and Science through funds provided by CICYT
[N] supported by the Natural Sciences and Engineering Research Council of Canada (NSERC)
[O] partially supported by the German Federal Ministry for Education and Research (BMBF)
[P] supported by RF Presidential grant N 4142.2010.2 for Leading Scientific Schools, by the Russian Ministry of Education and Science through its grant for Scientific Research on High Energy Physics and under contract No.02.740.11.0244
[Q] supported by the Netherlands Foundation for Research on Matter (FOM)
[R] supported by the Israel Science Foundation

[a] now at University of Salerno, Italy
[b] now at Queen Mary University of London, United Kingdom
[c] also funded by Max Planck Institute for Physics, Munich, Germany
[d] also Senior Alexander von Humboldt Research Fellow at Hamburg University, Institute of Experimental Physics, Hamburg, Germany
[e] also at Cracow University of Technology, Faculty of Physics, Mathemathics and Applied Computer Science, Poland
[f] supported by the research grant No. 1 P03B 04529 (2005-2008)
[g] now at Rockefeller University, New York, NY 10065, USA
[h] now at DESY group FS-CFEL-1
[i] now at Institute of High Energy Physics, Beijing, China
[j] now at DESY group FEB, Hamburg, Germany
[k] also at Moscow State University, Russia
[l] now at University of Liverpool, United Kingdom
[m] now at CERN, Geneva, Switzerland
[n] also affiliated with Universtiy College London, UK
[o] now at Goldman Sachs, London, UK
[p] also at Institute of Theoretical and Experimental Physics, Moscow, Russia
[q] also at FPACS, AGH-UST, Cracow, Poland
[r] partially supported by Warsaw University, Poland
[s] now at Istituto Nucleare di Fisica Nazionale (INFN), Pisa, Italy
[t] now at Haase Energie Technik AG, Neumünster, Germany
[u] now at Department of Physics, University of Bonn, Germany
[v] now at Biodiversität und Klimaforschungszentrum (BiK-F), Frankfurt, Germany
[w] also affiliated with DESY, Germany
[x] also at University of Tokyo, Japan
[y] now at Kobe University, Japan
[z] supported by DESY, Germany
[†] deceased
[aa] member of National Technical University of Ukraine, Kyiv Polytechnic Institute, Kyiv, Ukraine
[ab] member of National University of Kyiv - Mohyla Academy, Kyiv, Ukraine
[ac] partly supported by the Russian Foundation for Basic Research, grant 11-02-91345-DFG_a
[ad] Alexander von Humboldt Professor; also at DESY and University of Oxford
[ae] STFC Advanced Fellow
[af] nee Korcsak-Gorzo
[ag] This material was based on work supported by the National Science Foundation, while working at the Foundation.
[ah] also at Max Planck Institute for Physics, Munich, Germany, External Scientific Member
[ai] now at Tokyo Metropolitan University, Japan
[aj] now at Nihon Institute of Medical Science, Japan

[ak] now at Osaka University, Osaka, Japan
[al] also at Łódź University, Poland
[am] member of Łódź University, Poland
[an] now at Department of Physics, Stockholm University, Stockholm, Sweden
[ao] also at Cardinal Stefan Wyszyński University, Warsaw, Poland

1 Introduction

Quantum chromodynamics (QCD) is based on the non-Abelian group SU(3) which induces the self-coupling of the gluons. Investigations of the triple-gluon vertex (TGV) were carried out at LEP [1, 2] using angular correlations in four-jet events from Z^0 hadronic decays. At HERA, the effects of the different colour configurations arising from the underlying gauge structure can be studied in a clean way in three-jet production in neutral current (NC) deep inelastic scattering (DIS) and photoproduction (γp). These measurements provide complementary information to that already obtained in e^+e^- annihilation since they are probing the gauge structure in a different environment, a hadron-induced reaction, and are sensitive to new colour configurations.

Neutral current DIS at high Q^2 ($Q^2 \gg \Lambda^2_{\rm QCD}$, where Q^2 is the virtuality of the exchanged photon) up to leading order (LO) in the strong coupling constant, α_s, proceeds as in the quark-parton model ($Vq \to q$, where $V = \gamma^*$ or Z^0) or via the boson-gluon fusion ($Vg \to q\bar{q}$) and QCD-Compton ($Vq \to qg$) processes. Photoproduction is studied at HERA by means of ep scattering at low four-momentum transfers ($Q^2 \approx 0$). In γp reactions, two types of QCD processes contribute to jet production at LO [3, 4]: either the photon interacts directly with a parton in the proton (the direct process) or the photon acts as a source of partons which scatter off those in the proton (the resolved process).

A subset of resolved subprocesses with two jets in the final state are described by diagrams with a TGV; however, such events are difficult to distinguish from two-jet events without such a contribution. Three-jet final states in direct γp processes also contain contributions from TGVs and are easier to identify. Since three-jet production in NC DIS proceeds via the same diagrams as in direct γp, such processes can also be used to investigate the underlying gauge symmetry. Examples of diagrams contributing to the four colour configurations are shown in Fig. 1: (A) double-gluon bremsstrahlung from a quark line, (B) the splitting of a virtual gluon into a pair of final-state gluons, (C) the production of a $q\bar{q}$ pair through the exchange of a virtual gluon emitted by an incoming quark, and (D) the production of a $q\bar{q}$ pair through the exchange of a virtual gluon arising from the splitting of an incoming gluon.

Other possible diagrams and interferences correspond to one of the four configurations. The production rate of all contributions is proportional to the so-called colour factors, C_F, C_A and T_F, which are a physical manifestation of the underlying group structure. For QCD, these factors represent the relative strengths of the processes $q \to qg$, $g \to gg$ and $g \to q\bar{q}$. The contributions of the diagrams of Fig. 1 are proportional to C_F^2, $C_F C_A$, $C_F T_F$ and $T_F C_A$, respectively, independently of the underlying gauge symmetry. It should be noted that the $T_F C_A$ contribution, which arises from gluon-induced processes, is not present in e^+e^- annihilation and is investigated here for the first time.

Three-jet cross sections were previously measured in γp [5] and in NC DIS [6, 7]. The shape of the measured cross sections was well reproduced by perturbative QCD (pQCD) calculations and a value of α_s was extracted [6]. In this paper, measurements of angular correlations in three-jet events in γp and NC DIS are presented. The comparison between the measurements and

fixed-order $\mathcal{O}(\alpha_s^2)$ and $\mathcal{O}(\alpha_s^3)$ perturbative calculations based on different colour configurations provides a stringent test of pQCD predictions directly beyond LO and gives insight into the underlying group symmetry. Phase-space regions where the angular correlations show potential sensitivity to the presence of the TGV were identified.

2 Theoretical framework

The dynamics of a gauge theory such as QCD are completely defined by the commutation relations between its group generators T^i,

$$[T^i, T^j] = i \sum_k f^{ijk} \cdot T^k,$$

where f^{ijk} are the structure constants. The generators T^i can be represented as matrices. In perturbative calculations, the average (sum) over all possible colour configurations in the initial (final) states leads to the appearance of combinatoric factors C_F, C_A and T_F, which are defined by the relations

$$\sum_{k,\eta} T^k_{\alpha\eta} T^k_{\eta\beta} = \delta_{\alpha\beta} C_F, \ \sum_{j,k} f^{jkm} f^{jkn} = \delta^{mn} C_A,$$

$$\sum_{\alpha,\beta} T^m_{\alpha\beta} T^n_{\beta\alpha} = \delta^{mn} T_F.$$

Measurements of the ratios between the colour factors allow the experimental determination of the underlying gauge symmetry of the strong interactions. For SU(N), the predicted values of the colour factors are:

$$C_A = N, \ \ C_F = \frac{N^2 - 1}{2N} \ \text{ and } \ T_F = 1/2,$$

where N is the number of colour charges. In particular, SU(3) predicts $C_A/C_F = 9/4$ and $T_F/C_F = 3/8$. In contrast, an Abelian gluon theory based on U$(1)^3$ would predict $C_A/C_F = 0$ and $T_F/C_F = 3$. A non-Abelian theory based on SO(3) predicts $C_A/C_F = 1$ and $T_F/C_F = 1$.

The $\mathcal{O}(\alpha_s^2)$ calculations of three-jet cross sections for direct γp and NC DIS processes can be expressed in terms of C_A, C_F and T_F as [8]:

$$\sigma_{ep\to 3\text{jets}} = C_F^2 \cdot \sigma_A + C_F C_A \cdot \sigma_B + C_F T_F \cdot \sigma_C + T_F C_A \cdot \sigma_D, \tag{1}$$

where σ_A, ..., σ_D are the partonic cross sections for the different contributions (see Fig. 1).

3 Definition of the angular correlations

Angular-correlation observables were devised to distinguish the contributions from the different colour configurations. They are defined in terms of the three jets with highest transverse energy in an event and the beam direction as:

- $\boldsymbol{\theta_H}$, the angle between the plane determined by the highest-transverse-energy jet and the beam and the plane determined by the two jets with the second-highest and third-highest transverse energy [9]. For three-jet events in ep collisions, the variable θ_H was designed [9] to be sensitive to the TGV in quark-induced processes (see Fig. 1B);

- $\boldsymbol{\alpha_{23}}$, the angle between the two lowest-transverse-energy jets; the jets are ordered according to decreasing transverse energy. This variable is based on the angle $\alpha_{34}^{e^+e^-}$ for $e^+e^- \to$ 4 jets [2], which distinguishes between contributions from double-bremsstrahlung diagrams and diagrams involving the TGV;

- $\boldsymbol{\beta_{\mathrm{KSW}}}$, the angle defined via the equation
$$\cos(\beta_{\mathrm{KSW}}) = \cos\left[\tfrac{1}{2}\left(\angle[(\vec{p}_1 \times \vec{p}_3),(\vec{p}_2 \times \vec{p}_B)] + \angle[(\vec{p}_1 \times \vec{p}_B),(\vec{p}_2 \times \vec{p}_3)]\right)\right],$$
where $\vec{p}_i,\ i = 1,...,3$ is the momentum of jet i and $\vec{p}_B$ is a unit vector in the direction of the proton beam. This variable is based on the Körner-Schierholz-Willrodt angle $\Phi_{\mathrm{KSW}}^{e^+e^-}$ for $e^+e^- \to 4$ jets [10], which is sensitive to the differences between $q\bar{q}gg$ and $q\bar{q}q\bar{q}$ final states;

- $\boldsymbol{\eta_{\mathrm{max}}^{\mathrm{jet}}}$, the maximum pseudorapidity[1] of the three jets.

4 Experimental set-up

The data samples used in this analysis were collected with the ZEUS detector at HERA and correspond to an integrated luminosity of 44.9 ± 0.8 (65.1 ± 1.5) pb^{-1} for e^+p collisions taken during 1995–97 (1999–2000) and 16.7 ± 0.3 pb^{-1} for e^-p collisions taken during 1998–99. During 1995–97 (1998–2000), HERA operated with protons of energy $E_p = 820$ (920) GeV and positrons or electrons[2] of energy $E_e = 27.5$ GeV, yielding a centre-of-mass energy of $\sqrt{s} = 300$ (318) GeV.

A detailed description of the ZEUS detector can be found elsewhere [11, 12]. A brief outline of the components that are most relevant for this analysis is given below. Charged particles were tracked in the central tracking detector (CTD) [13], which operated in a magnetic field of

[1] The ZEUS coordinate system is a right-handed Cartesian system, with the Z axis pointing in the proton beam direction, referred to as the "forward direction", and the X axis pointing towards the centre of HERA. The coordinate origin is at the nominal interaction point. The pseudorapidity is defined as $\eta = -\ln(\tan\frac{\theta}{2})$, where the polar angle θ is taken with respect to the proton beam direction.

[2] Here and in the following, the term "electron" denotes generically both the electron (e^-) and the positron (e^+).

1.43 T provided by a thin superconducting solenoid. The CTD consisted of 72 cylindrical drift-chamber layers, organised in nine superlayers covering the polar-angle region $15^\circ < \theta < 164^\circ$. The transverse-momentum resolution for full-length tracks was parameterised as $\sigma(p_T)/p_T = 0.0058p_T \oplus 0.0065 \oplus 0.0014/p_T$, with p_T in GeV. The tracking system was used to measure the interaction vertex with a typical resolution along (transverse to) the beam direction of 0.4 (0.1) cm and to cross-check the energy scale of the calorimeter.

The high-resolution uranium–scintillator calorimeter (CAL) [14] covered 99.7% of the total solid angle and consisted of three parts: the forward (FCAL), the barrel (BCAL) and the rear (RCAL) calorimeters. Each part was subdivided transversely into towers and longitudinally into one electromagnetic section (EMC) and either one (in RCAL) or two (in BCAL and FCAL) hadronic sections (HAC). The smallest subdivision of the calorimeter was called a cell. Under test-beam conditions, the CAL single-particle relative energy resolutions were $\sigma(E)/E = 0.18/\sqrt{E}$ for electrons and $\sigma(E)/E = 0.35/\sqrt{E}$ for hadrons, with E in GeV.

The luminosity was measured from the rate of the bremsstrahlung process $ep \to e\gamma p$. The resulting small-angle energetic photons were measured by the luminosity monitor [15], a lead–scintillator calorimeter placed in the HERA tunnel at $Z = -107$ m.

5 Data selection and jet search

A three-level trigger system was used to select events online [12, 16]. At the third level, jets were reconstructed using the energies and positions of the CAL cells. Events with at least one (two) jet(s) with transverse energy in excess of 10 (6) GeV and pseudorapidity below 2.5 were accepted. For trigger-efficiency studies, no jet algorithm was applied and events with a total transverse energy, excluding the energy in the eight CAL towers immediately surrounding the forward beampipe, of at least 25 GeV were selected in the γp sample; for the NC DIS sample, events were selected in which the scattered-electron candidate was identified using localised energy depositions in the CAL.

In the offline selection, a reconstructed event vertex consistent with the nominal interaction position was required and cuts based on tracking information were applied to reduce the contamination from beam-induced and cosmic-ray background events. The selection criteria of the γp and NC DIS samples were analogous to previous publications [17, 18].

The selected γp sample, based on the 1995–2000 data, consisted of events from ep interactions with $Q^2 < 1$ GeV^2 and a median $Q^2 \approx 10^{-3}$ GeV^2. The event sample was restricted to the kinematic range $0.2 < y < 0.85$, where y is the inelasticity.

The k_T cluster algorithm [19] was used in the longitudinally invariant inclusive mode [20] to reconstruct jets in the measured hadronic final state from the energy deposits in the CAL cells (calorimetric jets). The axis of the jet was defined according to the Snowmass convention [21].

For γp events, the jet search was performed in the $\eta - \phi$ plane of the laboratory frame. Corrections [17, 22] to the jet transverse energy, E_T^{jet}, were applied to the calorimetric jets as a function

of the jet pseudorapidity, $\eta^{\rm jet}$, and $E_T^{\rm jet}$ and averaged over the jet azimuthal angle. Events with at least three jets of $E_T^{\rm jet} > 14$ GeV and $-1 < \eta^{\rm jet} < 2.5$ were retained. Direct γp events were further selected by requiring $x_\gamma^{\rm obs} > 0.8$, where $x_\gamma^{\rm obs}$, the fraction of the photon momentum participating in the production of the three jets with highest $E_T^{\rm jet}$, is defined as

$$x_\gamma^{\rm obs} = \frac{1}{2yE_e}\left(E_T^{\rm jet1}e^{-\eta^{\rm jet1}} + E_T^{\rm jet2}e^{-\eta^{\rm jet2}} + E_T^{\rm jet3}e^{-\eta^{\rm jet3}}\right).$$

The final γp data sample contained 1888 events.

Events from NC DIS interactions were selected from the 1998–2000 data. Two samples were studied: $Q^2 > 125$ GeV^2 and $500 < Q^2 < 5000$ GeV^2. For both samples, $|\cos\gamma_h|$ was restricted to be below 0.65, where γ_h, which corresponds to the angle of the scattered quark in the quark-parton model, is defined as

$$\cos\gamma_h = \frac{(1-y)xE_p - yE_e}{(1-y)xE_p + yE_e}$$

and x is the Bjorken variable.

For NC DIS events, the k_T jet algorithm was applied after excluding those cells associated with the scattered-electron candidate and the search was conducted in the Breit frame. The Breit frame [23] is the frame in which the exchanged virtual boson is purely space-like, with 3-momentum $\boldsymbol{q} = (0, 0, -Q)$, providing a maximal separation between the products of the beam fragmentation and the hard interaction. Jet transverse-energy corrections were computed using the method developed in a previous analysis [18,24]. Events were required to have at least three jets satisfying $E_{T,\rm B}^{\rm jet1} > 8$ GeV, $E_{T,\rm B}^{\rm jet2,3} > 5$ GeV and $-2 < \eta_{\rm B}^{\rm jet} < 1.5$, where $E_{T,\rm B}^{\rm jet}$ and $\eta_{\rm B}^{\rm jet}$ are the jet transverse energy and pseudorapidity in the Breit frame, respectively. The final NC DIS data sample with $Q^2 > 125$ ($500 < Q^2 < 5000$) GeV^2 contained 1095 (492) events.

6 Monte Carlo simulation

Samples of Monte Carlo (MC) events were generated to determine the response of the detector to jets of hadrons and the correction factors necessary to obtain the hadron-level jet cross sections. The hadron level is defined by those hadrons with lifetime $\tau \geq 10$ ps. For the NC DIS sample, the MC events were also used to correct the measured cross sections for QED radiative effects and the running of $\alpha_{\rm em}$.

The generated events were passed through the GEANT 3.13-based [25] ZEUS detector- and trigger-simulation programs [12]. They were reconstructed and analysed by the same program chain as the data. The k_T jet algorithm was applied to the MC simulated events using the CAL cells in the same way as for the data. The jet algorithm was also applied to the final-state particles (hadron level) and the partons available after the parton shower (parton level).

The programs PYTHIA 6.1 [26] and HERWIG 6.1 [27] were used to generate γp events for resolved and direct processes. Events were generated using GRV-HO [28] for the photon and CTEQ4M [29] for the proton parton distribution functions (PDFs). In both generators, the partonic processes are simulated using LO matrix elements, with the inclusion of initial- and final-state parton showers. Fragmentation into hadrons is performed using the Lund string model [30] as implemented in JETSET [26,31] in the case of PYTHIA, and a cluster model [32] in the case of HERWIG.

Neutral current DIS events including radiative effects were simulated using the HERACLES 4.6.1 [33] program with the DJANGOH 1.1 [34] interface to the hadronisation programs. HERACLES includes corrections for initial- and final-state radiation, vertex and propagator terms, and two-boson exchange. The QCD cascade is simulated using the colour-dipole model (CDM) [35] including the LO QCD diagrams as implemented in ARIADNE 4.08 [36]; additional samples were generated with the MEPS model of LEPTO 6.5 [37]. Both MC programs use the Lund string model for the hadronisation. The CTEQ5D [38] proton PDFs were used for these simulations.

7 Fixed-order calculations

The calculations of direct γp processes used in this analysis are based on the program by Klasen, Kleinwort and Kramer (KKK) [39]. The number of flavours was set to five; the renormalisation, μ_R, and factorisation scales, μ_F, were set to $\mu_R = \mu_F = E_T^{\max}$, where $E_T^{\max}$ is the highest E_T^{jet} in an event. The calculations were performed using the ZEUS-S [40] parameterisations of the proton PDFs; α_s was calculated at two loops using $\Lambda^{(5)}_{\overline{\text{MS}}} = 226$ MeV, which corresponds to $\alpha_s(M_Z) = 0.118$. These calculations are $\mathcal{O}(\alpha_s^2)$ and represent the lowest-order contribution to three-jet γp. Full $\mathcal{O}(\alpha_s^3)$ corrections are not yet available for three-jet cross sections in γp.

The calculations of NC DIS processes used in this analysis are based on the program NLOJET++ [41], which provides $\mathcal{O}(\alpha_s^2)$ and $\mathcal{O}(\alpha_s^3)$ predictions for three-jet cross sections. The scales were chosen to be $\mu_R = \mu_F = Q$. Other parameters were set as for the γp program.

In general, the programs mentioned above are very flexible and provide observable-independent computations that allow a complete analytical cancellation of the soft and collinear singularities encountered in the calculations of jet cross sections. However, these programs were written assuming the SU(3) gauge group and the different ingredients necessary to perform a calculation according to Eq. (1) were not readily available. The programs were rewritten in order to disentagle the colour components to make separate predictions for σ_A, ..., σ_D.

The k_T jet algorithm was applied to the partons in the events generated by KKK and NLOJET++ in order to compute the jet cross-section predictions. Thus, these predictions refer to jets of partons. Since the measurements refer to jets of hadrons, the calculations were corrected to the hadron level. The multiplicative correction factors, defined as the ratios between the cross section for jets of hadrons and that for jets of partons, were estimated using the MC samples described in Section 6. The normalised cross-section calculations (see Section 8 for the definition

of the cross sections) changed typically by less than ± 5 (10)% for the predictions in γp (NC DIS) upon application of the parton-to-hadron corrections. Therefore, the effect of the parton-to-hadron corrections on the angular distributions is small. In NC DIS processes, other effects not accounted for in the calculations, namely Z^0 exchange, were also corrected for using the MC samples.

The predictions for jet cross sections are expressed as the convolution of the PDFs and the matrix elements, which depend on α_s. Both the PDFs and α_s evolve with the energy scale. In the calculations performed for this analysis, QCD evolution via the DGLAP and the renormalisation group equations, respectively, were used. These evolution equations also depend on the colour factors. This procedure introduces an additional dependence on the colour factors with respect to that shown in Eq. (1); this dependence is suppressed by considering normalised cross sections. The remaining dependence was estimated by comparing to calculations with fixed μ_F or μ_R, i.e. no evolution of the PDFs or α_s was allowed. The values chosen for μ_F and μ_R were the mean values of the data distributions, $\langle E_T^{\rm max} \rangle_{\rm data} = 27.8$ GeV for γp and $\sqrt{\langle Q^2 \rangle_{\rm data}} = 31.3$ (36.6) GeV for NC DIS with $Q^2 > 125$ ($500 < Q^2 < 5000$) GeV^2.

Figure 2 shows the relative difference of the $\mathcal{O}(\alpha_s^2)$ γp normalised cross-section calculations with μ_F (μ_R) fixed[3] to those in which $\mu_F = E_T^{\rm max}$ ($\mu_R = E_T^{\rm max}$) as a function of the angular variables studied. Figures 3(a) and 3(b) show the same relative difference for the $\mathcal{O}(\alpha_s^2)$ NLOJET++ calculations for $Q^2 > 125$ GeV^2.

Very small differences are observed for the μ_F variation. Sizeable differences for the μ_R variation are seen in some regions; in particular, a trend is observed for the relative difference as a function of $\eta^{\rm jet}_{\rm max}$: this trend is due to the fact that the mean values of Q^2 in each bin of $\eta^{\rm jet}_{\rm max}$ increase as $\eta^{\rm jet}_{\rm max}$ decreases.

These studies demonstrate that the normalised cross sections have little sensitivity to the evolution of the PDFs. It should be noted that there is a remaining dependence on the colour factors through the relative contributions of quark- and gluon-induced processes as obtained in the extraction of the PDFs, in which the values of $SU(3)$ were assumed[4]. There is still some sensitivity to the running of α_s. Figures 3(c) and 3(d) show the relative difference for $500 < Q^2 < 5000$ GeV^2. The restriction of the phase space further reduces the dependence on the running of α_s; thus, this region is more suitable to extract the colour factors in NC DIS at $\mathcal{O}(\alpha_s^2)$. At $\mathcal{O}(\alpha_s^3)$ (see Figs. 3(e) to 3(h)), the effect due to the running of α_s is already very small for $Q^2 > 125$ GeV^2. Therefore, the wider phase-space region can be kept in an extraction of the colour factors at $\mathcal{O}(\alpha_s^3)$.

The following theoretical uncertainties were considered (as an example of the size of the uncertainties, an average value of the effect of each uncertainty on the normalised cross section as a function of θ_H is shown in parentheses for γp, NC DIS with $Q^2 > 125$ GeV^2 and NC DIS with

[3] When μ_F was fixed, μ_R was allowed to vary with the scale, and vice-versa.

[4] In order to consider that correlation, an extraction of the PDFs leaving the colour factors as free parameters would be necessary, a task which is beyond the scope of the present paper.

$500 < Q^2 < 5000$ GeV^2):

- the uncertainty in the modelling of the parton shower was estimated by using different models (see Section 6) to calculate the parton-to-hadron correction factors ($\pm 2.8\%$, $\pm 2.9\%$ and $\pm 5.8\%$);
- the uncertainty on the calculations due to higher-order terms was estimated by varying μ_R by a factor of two up and down ($^{+0.6}_{-0.8}\%$, $\pm 1.6\%$ and $\pm 2.2\%$);
- the uncertainty on the calculations due to those on the proton PDFs was estimated by repeating the calculations using 22 additional sets from the ZEUS analysis [40]; this analysis takes into account the statistical and correlated systematic experimental uncertainties of each data set used in the determination of the proton PDFs ($\pm 0.7\%$, $\pm 0.2\%$ and $\pm 0.1\%$);
- the uncertainty on the calculations due to that on $\alpha_s(M_Z)$ was estimated by repeating the calculations using two additional sets of proton PDFs, for which different values of $\alpha_s(M_Z)$ were assumed in the fits. The difference between the calculations using these various sets was scaled to reflect the uncertainty on the current world average of α_s [42] (negligible in all cases);
- the uncertainty of the calculations due to the choice of μ_F was estimated by varying μ_F by a factor of two up and down (negligible in all cases).

The total theoretical uncertainty was obtained by adding in quadrature the individual uncertainties listed above. The dominant source of theoretical uncertainty is that on the modelling of the parton shower, which is to a large extent correlated bin to bin.

8 Definition of the cross sections

Normalised differential three-jet cross sections were measured as functions of θ_H, α_{23} and β_{KSW} using the selected data samples in γp and NC DIS. For NC DIS, the normalised differential three-jet cross section as a function of $\eta^{\mathrm{jet}}_{\mathrm{max}}$ was also measured. The normalised differential three-jet cross section in bin i for an observable A was obtained using

$$\frac{1}{\sigma}\frac{d\sigma_i}{dA} = \frac{1}{\sigma}\frac{N_{\mathrm{data},i}}{\mathcal{L}\cdot\Delta A_i}\cdot\frac{N^{\mathrm{had}}_{\mathrm{MC},i}}{N^{\mathrm{det}}_{\mathrm{MC},i}},$$

where $N_{\mathrm{data},i}$ is the number of data events in bin i, $N^{\mathrm{had}}_{\mathrm{MC},i}$ ($N^{\mathrm{det}}_{\mathrm{MC},i}$) is the number of MC events at hadron (detector) level, $\mathcal{L}$ is the integrated luminosity and ΔA_i is the bin width. The integrated three-jet cross section, σ, was computed using the formula:

$$\sigma = \sum_i \frac{N_{\mathrm{data},i}}{\mathcal{L}}\cdot\frac{N^{\mathrm{had}}_{\mathrm{MC},i}}{N^{\mathrm{det}}_{\mathrm{MC},i}},$$

where the sum runs over all bins.

For the γp sample, due to the different centre-of-mass energies of the two data sets used in the analysis, the measured normalised differential three-jet cross sections were combined using

$$\sigma^{\text{comb}} = \frac{\sigma_{300} \cdot \mathcal{L}_{300} + \sigma_{318} \cdot \mathcal{L}_{318}}{\mathcal{L}_{300} + \mathcal{L}_{318}},$$

where $\mathcal{L}_{\sqrt{s}}$ is the luminosity and $\sigma_{\sqrt{s}}$ is the measured cross section corresponding to $\sqrt{s} = 300$ or 318 GeV. This formula was applied for combining the differential and total cross sections. The same formula was used for computing the $\mathcal{O}(\alpha_s^2)$ predictions in γp.

9 Acceptance corrections and experimental uncertainties

The Pythia (MEPS) MC samples were used to compute the acceptance corrections to the angular distributions of the γp (NC DIS) data. These correction factors took into account the efficiency of the trigger, the selection criteria and the purity and efficiency of the jet reconstruction. The samples of Herwig and CDM were used to compute the systematic uncertainties coming from the fragmentation and parton-shower models in γp and NC DIS, respectively.

The data E_T^{jet}, η^{jet} and x_γ^{obs} distributions of the γp sample, before the $x_\gamma^{\text{obs}} > 0.8$ requirement, are shown in Fig. 4 together with the MC simulations of Pythia and Herwig. Considering that three-jet events in the MC arise only from the parton-shower approximation, the description of the data is reasonable. Figure 4(d) shows the resolved and direct contributions for the Pythia MC separately. It is observed that the region of $x_\gamma^{\text{obs}} > 0.8$ is dominated by direct γp events. The remaining contribution in this region from resolved-photon events was estimated using Pythia (Herwig) simulated events to be ≈ 25 (31)%.

Figure 5 shows the data distributions as functions of θ_H, α_{23} and β_{KSW} together with the simulations of Pythia and Herwig for $x_\gamma^{\text{obs}} > 0.8$. The Pythia MC predictions describe the data distributions well, whereas the description given by Herwig is somewhat poorer. It was checked that the angular distributions of the events from resolved processes with $x_\gamma^{\text{obs}} > 0.8$ were similar to those from direct processes (see Fig. 5) and, therefore, no subtraction of the resolved processes was performed when comparing to the fixed-order calculations described in Section 7.

The data $E_{T,\text{B}}^{\text{jet1}}$, $E_{T,\text{B}}^{\text{jet2,3}}$, $\eta_{\text{B}}^{\text{jet}}$ and Q^2 distributions of the NC DIS samples are shown in Fig. 6 (7) for $Q^2 > 125$ ($500 < Q^2 < 5000$) GeV^2 together with the MC simulations from the MEPS and CDM models. Both models give a reasonably good description of the data in both kinematic regions. The data distributions of θ_H, α_{23}, β_{KSW} and $\eta_{\text{max}}^{\text{jet}}$ are shown in Fig. 8 (9) for $Q^2 > 125$ ($500 < Q^2 < 5000$) GeV^2. The MEPS MC predictions describe the data distributions well, whereas the description given by CDM is somewhat poorer.

A detailed study of the sources contributing to the experimental uncertainties was performed [43]. The following experimental uncertainties were considered for γp (as an example of the size of the uncertainties, an average value of the effect of each uncertainty on the cross section as a function of θ_H is shown in parentheses):

- the effect of the modelling of the parton shower and hadronisation was estimated by using HERWIG instead of PYTHIA to evaluate the correction factors ($\pm 6.1\%$);
- the effect of the uncertainty on the absolute energy scale of the calorimetric jets was estimated by varying $E_T^{\rm jet}$ in simulated events by its uncertainty of $\pm 1\%$. The method used was the same as in earlier publications [17, 18, 44] ($\pm 1.6\%$);
- the effect of the uncertainty on the reconstruction of y was estimated by varying its value in simulated events by the estimated uncertainty of $\pm 1\%$ ($\pm 1.0\%$);
- the effect of the uncertainty on the parameterisations of the proton and photon PDFs was estimated by using alternative sets of PDFs in the MC simulation to calculate the correction factors ($\pm 0.4\%$ and $\pm 2.0\%$, respectively);
- the uncertainty in the cross sections due to that in the simulation of the trigger ($\pm 0.4\%$).

For NC DIS events, the following experimental uncertainties were considered (as an example of the size of the uncertainties, an average value of the effect of each uncertainty on the cross section as a function of θ_H is shown in parentheses for the $Q^2 > 125$ GeV^2 and $500 < Q^2 < 5000$ GeV^2 kinematic regions):

- the effect of the modelling of the parton shower was estimated by using CDM instead of MEPS to evaluate the correction factors ($\pm 5.6\%$ and $\pm 9.1\%$);
- the effect of the uncertainty on the absolute energy scale of the calorimetric jets was estimated by varying $E_T^{\rm jet}$ in simulated events by its uncertainty of $\pm 1\%$ for $E_T^{\rm jet} > 10$ GeV and $\pm 3\%$ for lower $E_T^{\rm jet}$ values ($\pm 2.3\%$ and $\pm 1.7\%$);
- the uncertainties due to the selection cuts was estimated by varying the values of the cuts within the resolution of each variable (less than $\pm 1.6\%$ and less than $\pm 4.2\%$ in all cases);
- the uncertainty on the reconstruction of the boost to the Breit frame was estimated by using the direction of the track associated with the scattered electron instead of that derived from the impact position as determined from the energy depositions in the CAL ($\pm 1.6\%$ and $\pm 1.6\%$);
- the uncertainty in the absolute energy scale of the electron candidate was estimated to be $\pm 1\%$ [45] ($\pm 0.2\%$ and $\pm 0.3\%$);
- the uncertainty in the cross sections due to that in the simulation of the trigger ($\pm 0.5\%$ and $\pm 0.5\%$).

The dominant systematic effect comes from the modelling of the parton shower and hadronisation, which is to a large extent correlated bin to bin. Nevertheless, the effect of these uncertainties on the normalised differential three-jet cross sections is small compared to the statistical uncertainties for the measurements presented in Section 10. The systematic uncertainties were added in quadrature to the statistical uncertainties.

10 Results

Normalised differential three-jet cross sections were measured in γp in the kinematic region $Q^2 < 1$ GeV^2, $0.2 < y < 0.85$ and $x_\gamma^{\rm obs} > 0.8$. The cross sections were determined for jets of hadrons with $E_T^{\rm jet} > 14$ GeV and $-1 < \eta^{\rm jet} < 2.5$. In NC DIS, the cross sections were measured in two kinematic regimes: $Q^2 > 125$ GeV^2 and $500 < Q^2 < 5000$ GeV^2. In both cases, it was required that $|\cos\gamma_h| < 0.65$. The cross sections correspond to jets of hadrons with $E_{T,\rm B}^{\rm jet1} > 8$ GeV, $E_{T,\rm B}^{\rm jet2,3} > 5$ GeV and $-2 < \eta_{\rm B}^{\rm jet} < 1.5$.

10.1 Colour components and the triple-gluon vertex

Normalised differential three-jet cross sections at $\mathcal{O}(\alpha_s^2)$ of the individual colour components from Eq. (1), σ_A, ..., σ_D, were calculated using the programs described in Section 7 and are shown separately in Fig. 10 for γp and in Fig. 11 (12) for NC DIS with $Q^2 > 125$ ($500 < Q^2 < 5000$) GeV^2 as functions of the angular variables. In these and subsequent figures, the predictions were obtained by integrating over the same bins as for the data. The curves shown are a result of a cubic spline interpolation, except in the case of $\eta_{\rm max}^{\rm jet}$, for which a linear interpolation was used.

The component which contains the contribution from the TGV in quark-induced processes, σ_B, has a very different shape than the other components for all the angular variables considered, except for $\eta_{\rm max}^{\rm jet}$. The other components have distributions in $\beta_{\rm KSW}$ and θ_H that are similar and are best separated by the distribution of α_{23} in γp. In NC DIS with $500 < Q^2 < 5000$ GeV^2, the different colour components as functions of θ_H and $\beta_{\rm KSW}$ also display different shapes. In particular, the σ_D component, which also contains a TGV, shows a distinct shape for these distributions. This demonstrates that the three-jet angular correlations studied show sensitivity to the different colour components.

In γp (NC DIS: $Q^2 > 125$ GeV^2, $500 < Q^2 < 5000$ GeV^2), the SU(3)-based predictions for the relative contribution of each colour component to the total cross section are: (A): 0.13 (0.23, 0.30), (B): 0.10 (0.13, 0.14), (C): 0.45 (0.39, 0.35) and (D): 0.32 (0.25, 0.21). Therefore, the overall contribution from the diagrams that involve a TGV, B and D, amounts to 42 (38, 35)% in SU(3).

10.2 Three-jet cross sections in γp

The integrated three-jet cross section in γp in the kinematic range considered was measured to be:

$$\sigma_{ep\to 3\text{jets}} = 14.59 \pm 0.34 \text{ (stat.)} \, ^{+1.25}_{-1.31} \text{ (syst.) pb.}$$

The predicted $\mathcal{O}(\alpha_s^2)$ integrated cross section, which is the lowest order for this process and contains only direct processes, is $8.90 \, ^{+2.01}_{-2.92}$ pb.

The measured normalised differential three-jet cross sections are presented in Fig. 13 and Tables 1 to 3 as functions of θ_H, $\cos(\alpha_{23})$ and $\cos(\beta_{\text{KSW}})$. The measured cross section shows a peak at $\theta_H \approx 60^\circ$, increases as $\cos(\alpha_{23})$ increases and shows a broad peak in the range of $\cos(\beta_{\text{KSW}})$ between -0.5 to 0.1.

10.3 Three-jet cross sections in NC DIS

The integrated three-jet cross sections in NC DIS for $Q^2 > 125$ GeV^2 and $500 < Q^2 < 5000$ GeV^2 were measured to be:

$$\sigma_{ep\to 3\text{jets}} = 11.48 \pm 0.35 \text{ (stat.)} \ \pm 1.98 \text{ (syst.) pb}$$

and

$$\sigma_{ep\to 3\text{jets}} = 5.73 \pm 0.26 \text{ (stat.)} \ \pm 0.60 \text{ (syst.) pb.}$$

The predicted $\mathcal{O}(\alpha_s^3)$ integrated cross sections are 14.14 ± 3.40 pb and 6.86 ± 1.77 pb for the two kinematic regions, respectively.

The measured normalised differential three-jet cross sections in NC DIS for $Q^2 > 125$ GeV^2 and $500 < Q^2 < 5000$ GeV^2 are presented in Figs. 14 and 15, respectively, as functions of θ_H, $\cos(\alpha_{23})$, $\cos(\beta_{\text{KSW}})$ and $\eta^{\text{jet}}_{\text{max}}$ (see Tables 4 to 7). The measured cross sections have similar shapes in the two kinematic regions considered, except for the distribution as a function of $\cos(\beta_{\text{KSW}})$: the cross section decreases as $\cos(\beta_{\text{KSW}})$ increases for $500 < Q^2 < 5000$ GeV^2 whereas for $Q^2 > 125$ GeV^2 it shows an approximately constant behaviour for $-1 < \cos(\beta_{\text{KSW}}) < 0.25$. The measured cross section as a function of $\cos(\alpha_{23})$ peaks around 0.5 and increases as θ_H and $\eta^{\text{jet}}_{\text{max}}$ increase.

10.4 Comparison to fixed-order calculations

Calculations at $\mathcal{O}(\alpha_s^2)$ in which each colour contribution in Eq. (1) was weighted according to the colour factors predicted by SU(3) ($C_F = 4/3$, $C_A = 3$ and $T_F = 1/2$) are compared to the measurements in Figs. 13 to 17. The theoretical uncertainties are shown in Figs. 13, 16 and 17 as hatched bands. Since the calculations are normalised to unity, the uncertainties are

correlated among the points; this correlation is partially responsible for the pulsating pattern exhibited by the theoretical uncertainties. The predictions based on SU(3) give a reasonable description of the data for all angular correlations. For γp, the predictions do not include resolved processes (see Section 7), as calculations separated according to the different colour factors are not available. Monte Carlo simulations of such processes show that their contribution is most likely to be different from that of direct processes in the fifth and last bin of $(1/\sigma)(d\sigma/d\cos(\alpha_{23}))$ (see Figs. 5b and 13b).

To illustrate the sensitivity of the measurements to the colour factors, calculations based on different symmetry groups are also compared to the data in Figs. 13 to 15. In these calculations, the colour components were combined in such a way as to reproduce the colour structure of a theory based on the non-Abelian group SU(N) in the limit of large N ($C_F = 1$, $C_A = 2$ and $T_F = 0$), the Abelian group U(1)^3 ($C_F = 1$, $C_A = 0$ and $T_F = 3$), the non-Abelian group SO(3) ($C_F = 1/3$, $C_A = 3$ and $T_F = 1/3$) and, as an extreme choice, a calculation with $C_F = 0$. The shapes of the distributions predicted by U(1)^3 in γp are very similar to those by SU(3) due to the smallness of the component σ_B and the difficulty to distinguish the component σ_D. In NC DIS, the predictions of U(1)^3 show differences of around 10% with respect to those of SU(3), which are of the same order as the statistical uncertainties. In both regimes, the data clearly disfavour a theory based on SU(N) in the limit of large N or on $C_F = 0$.

Figures 16 and 17 show the measurements in NC DIS compared to the predictions of QCD at $\mathcal{O}(\alpha_s^2)$ and $\mathcal{O}(\alpha_s^3)$. This comparison provides a very stringent test of pQCD. The $\mathcal{O}(\alpha_s^3)$ calculations give a very good description of the data. In particular, a significant improvement in the description of the data can be observed for the first bin of the α_{23} distribution (Figs. 16b and 17b).

11 Summary and conclusions

Measurements of angular correlations in three-jet γp and NC DIS were performed in ep collisions at HERA using up to 127 pb^{-1} of data collected with the ZEUS detector. The cross sections refer to jets identified with the k_T cluster algorithm in the longitudinally invariant inclusive mode and selected with $E_T^{\rm jet} > 14$ GeV and $-1 < \eta^{\rm jet} < 2.5$ (γp) and $E_{T,\rm B}^{\rm jet1} > 8$ GeV, $E_{T,\rm B}^{\rm jet2,3} > 5$ GeV and $-2 < \eta_{\rm B}^{\rm jet} < 1.5$ (NC DIS). The measurements were made in the kinematic regions defined by $Q^2 < 1$ GeV^2, $0.2 < y < 0.85$ and $x_\gamma^{\rm obs} > 0.8$ (γp) and $Q^2 > 125$ GeV^2 or $500 < Q^2 < 5000$ GeV^2 and $|\cos\gamma_h| < 0.65$ (NC DIS). Normalised differential three-jet cross sections were measured as functions of θ_H, α_{23}, $\beta_{\rm KSW}$ and $\eta_{\rm max}^{\rm jet}$.

The colour configuration of the strong interaction was studied for the first time in ep collisions using the angular correlations in three-jet events. While the extraction of the colour factors will require the full analysis of all HERA data and complete $\mathcal{O}(\alpha_s^3)$ calculations, the studies presented in this paper demonstrate the potential of the method.

Fixed-order calculations separated according to the colour configurations were used to study

the sensitivity of the angular correlations to the underlying gauge structure. The predicted distributions of θ_H, α_{23} and β_{KSW} clearly isolate the contribution from the triple-gluon coupling in quark-induced processes while $\eta^{\mathrm{jet}}_{\mathrm{max}}$ isolates the contribution from gluon-induced processes. The variable α_{23} provides additional separation for the other contributions. Furthermore, the studies performed demonstrate that normalised cross sections in three-jet ep collisions have reduced sensitivity to the assumed evolution of the PDFs and the running of α_s.

The data clearly disfavour theories based on SU(N) in the limit of large N or $C_F = 0$. Differences between SU(3) and U(1)^3 are smaller than the current statistical uncertainties. The measurements are found to be consistent with the admixture of colour configurations as predicted by SU(3). The $\mathcal{O}(\alpha_s^3)$ calculations give a very good description of the NC DIS data.

Acknowledgments

We thank the DESY Directorate for their strong support and encouragement. We appreciate the contributions to the construction and maintenance of the ZEUS detector of many people who are not listed as authors. The HERA machine group and the DESY computing staff are especially acknowledged for their success in providing excellent operation of the collider and the data-analysis environment. We would like to thank M. Fontannaz, M. Klasen and Z. Nagy for useful discussions.

References

[1] ALEPH Coll., D. Decamp et al., Phys. Lett. **B 284**, 151 (1992);
ALEPH Coll., R. Barate et al., Z. Phys. **C 76**, 1 (1997);
ALEPH Coll., A. Heister et al., Eur. Phys. J. **C 27**, 1 (2003);
DELPHI Coll., P. Abreu et al., Z. Phys. **C 59**, 357 (1993);
DELPHI Coll., P. Abreu et al., Phys. Lett. **B 414**, 401 (1997);
DELPHI Coll., P. Abreu et al., Phys. Lett. **B 449**, 383 (1999);
L3 Coll., B. Adeva et al., Phys. Lett. **B 248**, 227 (1990);
OPAL Coll., M.Z. Akrawy et al., Z. Phys. **C 49**, 49 (1991);
OPAL Coll., R. Akers et al., Z. Phys. **C 65**, 367 (1995);
OPAL Coll., G. Abbiendi et al., Eur. Phys. J. **C 20**, 601 (2001).

[2] DELPHI Coll., P. Abreu et al., Phys. Lett. **B 255**, 466 (1991).

[3] C.H. Llewellyn Smith, Phys. Lett. **B 79**, 83 (1978);
I. Kang and C.H. Llewellyn Smith, Nucl. Phys. **B 166**, 413 (1980);
J.F. Owens, Phys. Rev. **D 21**, 54 (1980);
M. Fontannaz et al., Z. Phys. **C 6**, 241 (1980).

[4] W.J. Stirling and Z. Kunszt, *Proc. HERA Workshop*, R.D. Peccei (ed.), Vol. 1, p. 331. DESY, Hamburg, Germany (1987);
M. Drees and F. Halzen, Phys. Rev. Lett. **61**, 275 (1988);
M. Drees and R.M. Godbole, Phys. Rev. Lett. **61**, 682 (1988);
M. Drees and R.M. Godbole, Phys. Rev. **D 39**, 169 (1989);
H. Baer, J. Ohnemus and J.F. Owens, Z. Phys. **C 42**, 657 (1989);
H. Baer, J. Ohnemus and J.F. Owens, Phys. Rev. **D 40**, 2844 (1989).

[5] ZEUS Coll., J. Breitweg et al., Phys. Lett. **B 443**, 394 (1998);
ZEUS Coll., S. Chekanov et al., Nucl. Phys. **B 792**, 1 (2008).

[6] ZEUS Coll., S. Chekanov et al., Eur. Phys. J. **C 44**, 183 (2005).

[7] H1 Coll., C. Adloff et al., Phys. Lett. **B 515**, 17 (2001);
H1 Coll., F.D. Aaron et al., Eur. Phys. J. **C 65**, 363 (2010);
H1 Coll., F.D. Aaron et al., Eur. Phys. J. **C 67**, 1 (2010).

[8] P. Aurenche et al., Nucl. Phys. **B 286**, 553 (1987).

[9] R. Muñoz-Tapia and W.J. Stirling, Phys. Rev. **D 52**, 3894 (1995).

[10] J.G. Körner, G. Schierholz and J. Willrodt, Nucl. Phys. **B 185**, 365 (1981).

[11] ZEUS Coll., M. Derrick et al., Phys. Lett. **B 293**, 465 (1992).

[12] ZEUS Coll., U. Holm (ed.), *The ZEUS Detector*. Status Report (unpublished), DESY (1993), available on `http://www-zeus.desy.de/bluebook/bluebook.html`.

[13] N. Harnew et al., Nucl. Instr. and Meth. **A 279**, 290 (1989);
B. Foster et al., Nucl. Phys. Proc. Suppl. **B 32**, 181 (1993);
B. Foster et al., Nucl. Instr. and Meth. **A 338**, 254 (1994).

[14] M. Derrick et al., Nucl. Instr. and Meth. **A 309**, 77 (1991);
A. Andresen et al., Nucl. Instr. and Meth. **A 309**, 101 (1991);
A. Caldwell et al., Nucl. Instr. and Meth. **A 321**, 356 (1992);
A. Bernstein et al., Nucl. Instr. and Meth. **A 336**, 23 (1993).

[15] J. Andruszków et al., Preprint DESY-92-066, DESY, 1992;
ZEUS Coll., M. Derrick et al., Z. Phys. **C 63**, 391 (1994);
J. Andruszków et al., Acta Phys. Pol. **B 32**, 2025 (2001).

[16] W.H. Smith, K. Tokushuku and L.W. Wiggers, *Proc. Computing in High-Energy Physics (CHEP), Annecy, France, Sept. 1992*, C. Verkerk and W. Wojcik (eds.), p. 222. CERN, Geneva, Switzerland (1992). Also in preprint DESY 92-150B.

[17] ZEUS Coll., S. Chekanov et al., Phys. Lett. **B 560**, 7 (2003).

[18] ZEUS Coll., S. Chekanov et al., Phys. Lett. **B 649**, 12 (2007).

[19] S. Catani et al., Nucl. Phys. **B 406**, 187 (1993).

[20] S.D. Ellis and D.E. Soper, Phys. Rev. **D 48**, 3160 (1993).

[21] J.E. Huth et al., *Research Directions for the Decade. Proc. of Summer Study on High Energy Physics, 1990*, E.L. Berger (ed.), p. 134. World Scientific (1992). Also in preprint FERMILAB-CONF-90-249-E.

[22] C. Glasman, *Jet production at HERA with the ZEUS detector: resolved and direct processes in photoproduction and gluon content of the proton and the photon.* Ph.D. Thesis, Weizmann Institute of Science, 1995. DESY-F35D-95-02.

[23] R.P. Feynman, *Photon-Hadron Interactions.* Benjamin, New York, (1972);
K.H. Streng, T.F. Walsh and P.M. Zerwas, Z. Phys. C 2 (1979) 237.

[24] O. González, *Precise determinations of the strong coupling constant at HERA.* Ph.D. Thesis, Universidad Autónoma de Madrid, 2002. DESY-THESIS-2002-020.

[25] R. Brun et al., GEANT3, Technical Report CERN-DD/EE/84-1, CERN, 1987.

[26] T. Sjöstrand, Comp. Phys. Comm. **82**, 74 (1994);
T. Sjöstrand et al., Comp. Phys. Comm. **135**, 238 (2001).

[27] G. Marchesini et al., Comp. Phys. Comm. **67**, 465 (1992);
G. Corcella et al., JHEP **0101**, 010 (2001).

[28] M. Glück, E. Reya and A. Vogt, Phys. Rev. **D 45**, 3986 (1992);
M. Glück, E. Reya and A. Vogt, Phys. Rev. **D 46**, 1973 (1992).

[29] H.L. Lai et al., Phys. Rev. **D 55**, 1280 (1997).

[30] B. Andersson et al., Phys. Rep. **97**, 31 (1983).

[31] T. Sjöstrand, Comp. Phys. Comm. **39**, 347 (1986);
T. Sjöstrand and M. Bengtsson, Comp. Phys. Comm. **43**, 367 (1987).

[32] B.R. Webber, Nucl. Phys. **B 238**, 492 (1984).

[33] A. Kwiatkowski, H. Spiesberger and H.-J. Möhring, Comp. Phys. Comm. **69**, 155 (1992);
H. Spiesberger, *An Event Generator for ep Interactions at HERA Including Radiative Processes (Version 4.6)*, 1996, available on `http://www.desy.de/~hspiesb/heracles.html`.

[34] K. Charchuła, G.A. Schuler and H. Spiesberger, Comp. Phys. Comm. **81**, 381 (1994);
H. Spiesberger, HERACLES *and* DJANGOH*: Event Generation for ep Interactions at HERA Including Radiative Processes*, 1998, available on `http://wwwthep.physik.uni-mainz.de/~hspiesb/djangoh/djangoh.html`.

[35] Y. Azimov et al., Phys. Lett. **B 165**, 147 (1985);
G. Gustafson, Phys. Lett. **B 175**, 453 (1986);
G. Gustafson and U. Pettersson, Nucl. Phys. **B 306**, 746 (1988);
B. Andersson et al., Z. Phys. **C 43**, 625 (1989).

[36] L. Lönnblad, Comp. Phys. Comm. **71**, 15 (1992);
L. Lönnblad, Z. Phys. **C 65**, 285 (1995).

[37] G. Ingelman, A. Edin and J. Rathsman, Comp. Phys. Comm. **101**, 108 (1997).

[38] H.L. Lai et al., Eur. Phys. J. **C 12**, 375 (2000).

[39] M. Klasen, T. Kleinwort and G. Kramer, Eur. Phys. J. Direct **C 1**, 1 (1998).

[40] ZEUS Coll., S. Chekanov et al., Phys. Rev. **D 67**, 012007 (2003).

[41] Z. Nagy and Z. Trocsanyi, Phys. Rev. Lett. **87**, 082001 (2001).

[42] S. Bethke, J. Phys. **G 26**, R27 (2000). Updated in S. Bethke, Eur. Phys. J. **C 64** (2009) 689.

[43] M. Jiménez, *Tests of color dynamics and precision measurements of α_s using jet production in DIS with the ZEUS detector at HERA*. Ph.D. Thesis, Universidad Autónoma de Madrid, Spain, 2008. (Unpublished).

[44] M. Wing (on behalf of the ZEUS Coll.), *Proc. of the 10th International Conference on Calorimetry in High Energy Physics*, R. Zhu (ed.), p. 767. Pasadena, USA (2002). Also in preprint hep-ex/0206036.

[45] ZEUS Coll., S. Chekanov et al., Eur. Phys. J. **C 21**, 443 (2001).

θ_H bin (deg)	$(1/\sigma)\ d\sigma/d\theta_H$	$\delta_{\rm stat}$	$\delta_{\rm syst}$	$C_{\rm had}$
0, 9	0.00264	0.00038	± 0.00052	0.93
9, 18	0.00393	0.00044	± 0.00021	0.94
18, 27	0.00507	0.00051	$^{+0.00040}_{-0.00039}$	1.00
27, 36	0.00838	0.00064	$^{+0.00105}_{-0.00104}$	0.93
36, 45	0.01071	0.00075	± 0.00023	0.96
45, 54	0.01486	0.00087	$^{+0.00021}_{-0.00016}$	0.94
54, 63	0.01795	0.00098	$^{+0.00036}_{-0.00035}$	0.95
63, 72	0.01765	0.00095	± 0.00062	0.94
72, 81	0.01517	0.00088	$^{+0.00081}_{-0.00084}$	0.94
81, 90	0.01473	0.00086	$^{+0.00075}_{-0.00077}$	0.96

Table 1: *Normalised differential ep cross section for three-jet photoproduction integrated over $E_T^{\rm jet} > 14\ GeV$ and $-1 < \eta^{\rm jet} < 2.5$ in the kinematic region defined by $Q^2 < 1\ GeV^2$, $0.2 < y < 0.85$ and $x_\gamma^{\rm obs} > 0.8$ as a function of θ_H. The statistical and systematic uncertainties are shown separately. The multiplicative corrections for hadronisation effects to be applied to the parton-level QCD differential cross section, $C_{\rm had}$, are shown in the last column.*

$\cos(\alpha_{23})$ bin	$(1/\sigma)\ d\sigma/d\cos(\alpha_{23})$	$\delta_{\rm stat}$	$\delta_{\rm syst}$	$C_{\rm had}$
-1, -0.8	0.0138	0.0046	± 0.00042	1.04
-0.8, -0.6	0.078	0.012	$^{+0.004}_{-0.003}$	0.96
-0.6, -0.4	0.198	0.022	$^{+0.026}_{-0.027}$	0.95
-0.4, -0.2	0.343	0.029	$^{+0.041}_{-0.040}$	0.93
-0.2, 0	0.360	0.029	± 0.010	0.97
0, 0.2	0.512	0.034	$^{+0.014}_{-0.013}$	0.98
0.2, 0.4	0.618	0.037	$^{+0.015}_{-0.016}$	1.00
0.4, 0.6	0.847	0.044	± 0.013	0.99
0.6, 0.8	0.937	0.045	$^{+0.043}_{-0.042}$	0.99
0.8, 1	1.092	0.049	$^{+0.019}_{-0.018}$	1.02

Table 2: *Normalised differential ep cross section for three-jet photoproduction integrated over $E_T^{\rm jet} > 14\ GeV$ and $-1 < \eta^{\rm jet} < 2.5$ in the kinematic region defined by $Q^2 < 1\ GeV^2$, $0.2 < y < 0.85$ and $x_\gamma^{\rm obs} > 0.8$ as a function of $\cos(\alpha_{23})$. Other details as in the caption to Table 1.*

$\cos(\beta_{\rm KSW})$ bin	$(1/\sigma)\ d\sigma/d\cos(\beta_{\rm KSW})$	$\delta_{\rm stat}$	$\delta_{\rm syst}$	$C_{\rm had}$
-1, -0.8	0.552	0.035	± 0.044	0.97
-0.8, -0.6	0.651	0.039	± 0.026	0.99
-0.6, -0.4	0.745	0.042	$^{+0.032}_{-0.031}$	0.97
-0.4, -0.2	0.741	0.042	± 0.039	0.93
-0.2, 0	0.784	0.042	$^{+0.014}_{-0.016}$	0.96
0, 0.2	0.768	0.042	± 0.046	0.95
0.2, 0.4	0.500	0.034	± 0.005	0.94
0.4, 0.6	0.200	0.022	± 0.021	0.95
0.6, 0.8	0.056	0.010	$^{+0.010}_{-0.009}$	0.85
0.8, 1	0.0029	0.0015	± 0.0037	0.74

Table 3: *Normalised differential ep cross section for three-jet photoproduction integrated over $E_T^{\rm jet} > 14$ GeV and $-1 < \eta^{\rm jet} < 2.5$ in the kinematic region defined by $Q^2 < 1$ GeV^2, $0.2 < y < 0.85$ and $x_\gamma^{\rm obs} > 0.8$ as a function of $\cos(\beta_{\rm KSW})$. Other details as in the caption to Table 1.*

θ_H bin (deg)	$(1/\sigma)\ d\sigma/d\theta_H$	$\delta_{\rm stat}$	$\delta_{\rm syst}$	$C_{\rm QED}$	$C_{\rm had}$
$Q^2 > 125$ GeV^2					
0, 18	0.00372	0.00046	± 0.00031	0.92	0.89
18, 36	0.00770	0.00056	± 0.00095	0.88	0.90
36, 54	0.01291	0.00072	± 0.00045	0.96	0.84
54, 72	0.01438	0.00074	± 0.00042	1.00	0.84
72, 90	0.01686	0.00077	± 0.00160	0.99	0.84
$500 < Q^2 < 5000$ GeV^2					
0, 18	0.00481	0.00076	± 0.00048	0.88	0.92
18, 36	0.00993	0.00094	± 0.00231	0.95	0.96
36, 54	0.0141	0.0011	± 0.0004	0.92	0.97
54, 72	0.0134	0.0011	± 0.0008	1.03	0.89
72, 90	0.0133	0.0011	± 0.0023	0.96	0.94

Table 4: *Normalised differential ep cross section for three-jet production in NC DIS integrated over $E_{T,\rm B}^{\rm jet1} > 8$ GeV, $E_{T,\rm B}^{\rm jet2,3} > 5$ GeV and $-2 < \eta_{\rm B}^{\rm jet} < 1.5$ in the kinematic region given by $|\cos\gamma_h| < 0.65$ and $Q^2 > 125$ GeV^2 or $500 < Q^2 < 5000$ GeV^2 as a function of θ_H. The multiplicative corrections applied to the differential measured cross section to correct for QED radiative effects, $C_{\rm QED}$, is also shown. The multiplicative corrections for hadronisation effects and the Z^0-exchange contribution to be applied to the parton-level QCD differential cross section, $C_{\rm had}$, are shown in the last column. Other details as in the caption to Table 1.*

$\cos(\alpha_{23})$ bin	$(1/\sigma)\ d\sigma/d\cos(\alpha_{23})$	$\delta_{\rm stat}$	$\delta_{\rm syst}$	$C_{\rm QED}$	$C_{\rm had}$
$Q^2 > 125$ GeV^2					
-1, -0.6	0.117	0.015	$\pm$0.025	0.96	0.90
-0.6, -0.2	0.338	0.028	$\pm$0.035	1.01	0.70
-0.2, 0.2	0.568	0.032	$\pm$0.018	0.90	0.78
0.2, 0.6	0.993	0.037	$\pm$0.021	0.95	0.88
0.6, 1	0.484	0.030	$\pm$0.020	1.02	1.01
$500 < Q^2 < 5000$ GeV^2					
-1, -0.6	0.199	0.030	$\pm$0.018	1.04	0.83
-0.6, -0.2	0.381	0.043	$\pm$0.041	0.97	0.75
-0.2, 0.2	0.589	0.047	$\pm$0.074	0.92	0.83
0.2, 0.6	1.018	0.055	$\pm$0.061	0.95	1.07
0.6, 1	0.313	0.036	$\pm$0.022	0.97	1.16

Table 5: *Normalised differential ep cross section for three-jet production in NC DIS integrated over $E_{T,\rm B}^{\rm jet1} > 8$ GeV, $E_{T,\rm B}^{\rm jet2,3} > 5$ GeV and $-2 < \eta_{\rm B}^{\rm jet} < 1.5$ in the kinematic region given by $|\cos\gamma_h| < 0.65$ and $Q^2 > 125$ GeV^2 or $500 < Q^2 < 5000$ GeV^2 as a function of $\cos(\alpha_{23})$. Other details as in the caption to Table 4.*

$\cos(\beta_{\rm KSW})$ bin	$(1/\sigma)\ d\sigma/d\cos(\beta_{\rm KSW})$	$\delta_{\rm stat}$	$\delta_{\rm syst}$	$C_{\rm QED}$	$C_{\rm had}$
$Q^2 > 125$ GeV^2					
-1, -0.6	0.585	0.031	$\pm$0.057	0.92	0.95
-0.6, -0.2	0.691	0.034	$\pm$0.094	0.99	0.88
-0.2, 0.2	0.721	0.035	$\pm$0.020	1.01	0.85
0.2, 0.6	0.332	0.026	$\pm$0.025	0.92	0.74
0.6, 1	0.171	0.020	$\pm$0.022	0.93	0.71
$500 < Q^2 < 5000$ GeV^2					
-1, -0.6	0.770	0.052	$\pm$0.076	0.94	1.04
-0.6, -0.2	0.536	0.045	$\pm$0.112	0.93	0.97
-0.2, 0.2	0.497	0.045	$\pm$0.037	1.01	0.94
0.2, 0.6	0.430	0.044	$\pm$0.058	1.01	0.84
0.6, 1	0.267	0.036	$\pm$0.061	0.89	0.78

Table 6: *Normalised differential ep cross section for three-jet production in NC DIS integrated over $E_{T,\rm B}^{\rm jet1} > 8$ GeV, $E_{T,\rm B}^{\rm jet2,3} > 5$ GeV and $-2 < \eta_{\rm B}^{\rm jet} < 1.5$ in the kinematic region given by $|\cos\gamma_h| < 0.65$ and $Q^2 > 125$ GeV^2 or $500 < Q^2 < 5000$ GeV^2 as a function of $\cos(\beta_{\rm KSW})$. Other details as in the caption to Table 4.*

$\eta^{\rm jet}_{\rm max}$ bin	$(1/\sigma)\ d\sigma/d\eta^{\rm jet}_{\rm max}$	$\delta_{\rm stat}$	$\delta_{\rm syst}$	$C_{\rm QED}$	$C_{\rm had}$
$Q^2 > 125$ GeV^2					
-2, -0.1	0.0042	0.0013	$\pm$0.0006	1.07	0.61
-0.1, 0.3	0.092	0.016	$\pm$0.012	1.17	0.77
0.3, 0.7	0.267	0.024	$\pm$0.054	0.96	0.81
0.7, 1.1	0.751	0.034	$\pm$0.016	0.93	0.83
1.1, 1.5	1.370	0.038	$\pm$0.048	0.96	0.88
$500 < Q^2 < 5000$ GeV^2					
-2, -0.1	0.0059	0.0021	$\pm$0.0022	1.14	0.62
-0.1, 0.3	0.110	0.022	$\pm$0.011	0.96	0.77
0.3, 0.7	0.378	0.040	$\pm$0.084	0.96	0.86
0.7, 1.1	0.918	0.054	$\pm$0.052	0.93	0.93
1.1, 1.5	1.066	0.056	$\pm$0.035	0.98	1.00

Table 7: *Normalised differential ep cross section for three-jet production in NC DIS integrated over* $E^{\rm jet1}_{T,{\rm B}} > 8$ *GeV,* $E^{\rm jet2,3}_{T,{\rm B}} > 5$ *GeV and* $-2 < \eta^{\rm jet}_{\rm B} < 1.5$ *in the kinematic region given by* $|\cos\gamma_h| < 0.65$ *and* $Q^2 > 125$ *GeV*^{2} *or* $500 < Q^2 < 5000$ *GeV*^{2} *as a function of* $\eta^{\rm jet}_{\rm max}$*. Other details as in the caption to Table 4.*

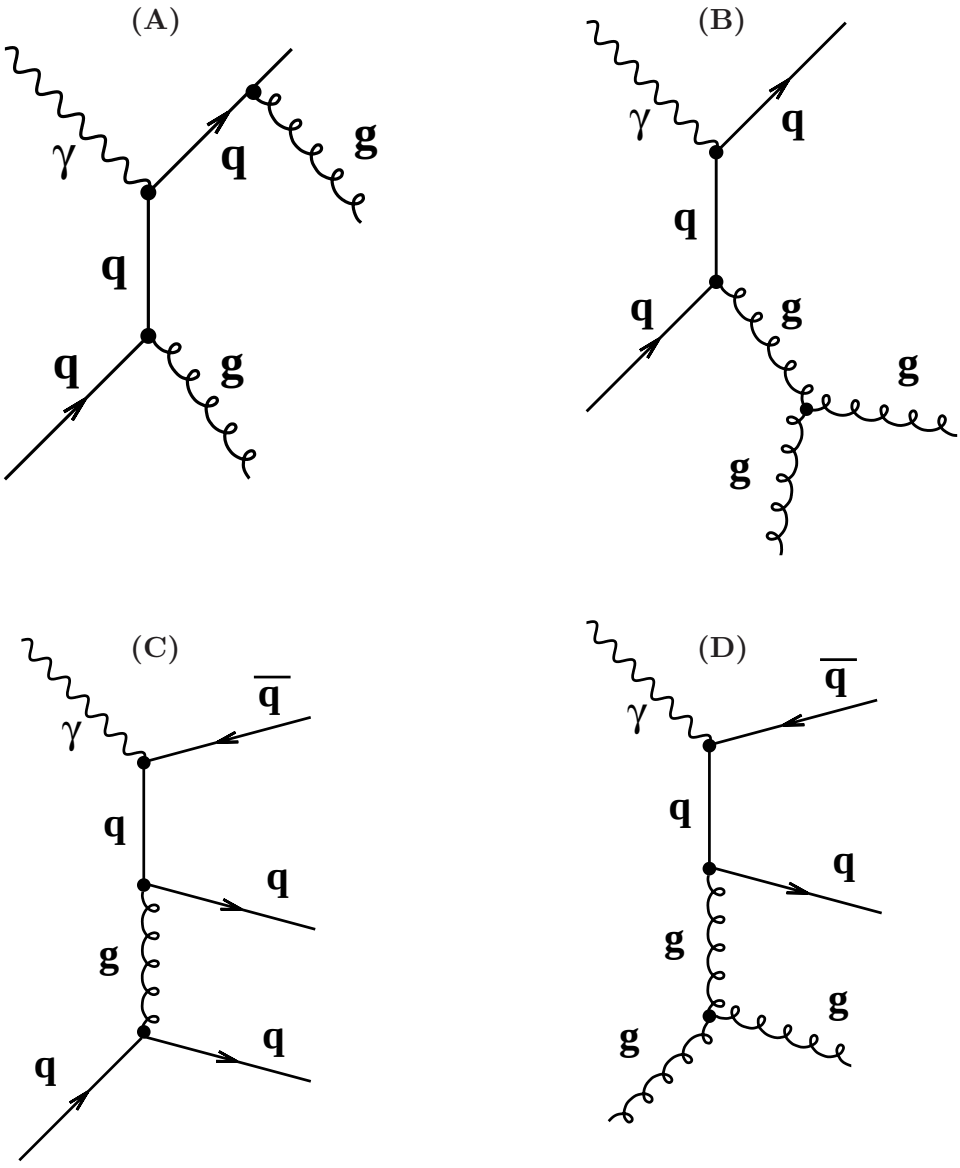

Figure 1: *Examples of diagrams for the photoproduction of three-jet events through direct-photon processes and in NC DIS three-jet events in each colour configuration: (A) double-gluon bremsstrahlung from a quark line; (B) the splitting of a virtual gluon into a pair of final-state gluons; (C) the production of a $q\bar{q}$ pair through the exchange of a virtual gluon emitted by an incoming quark; (D) the production of a $q\bar{q}$ pair through the exchange of a virtual gluon arising from the splitting of an incoming gluon.*

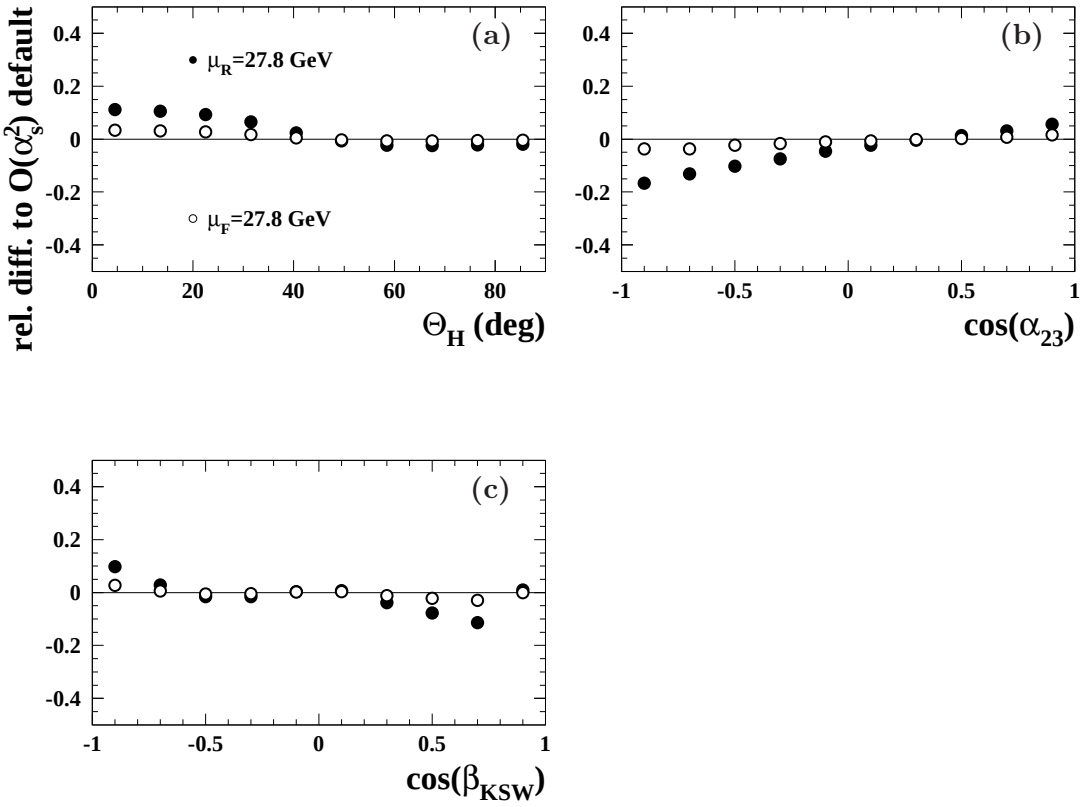

Figure 2: *Relative difference between the $\mathcal{O}(\alpha_s^2)$ normalised cross-section calculations with $\mu_R = 27.8$ GeV and the calculations with $\mu_R = E_T^{\max}$ (dots) and between the $\mathcal{O}(\alpha_s^2)$ calculations with $\mu_F = 27.8$ GeV and the calculations with $\mu_F = E_T^{\max}$ (open circles) in γp as functions of (a) θ_H, (b) $\cos(\alpha_{23})$ and (c) $\cos(\beta_{\rm KSW})$. These calculations do not include corrections for hadronisation effects.*

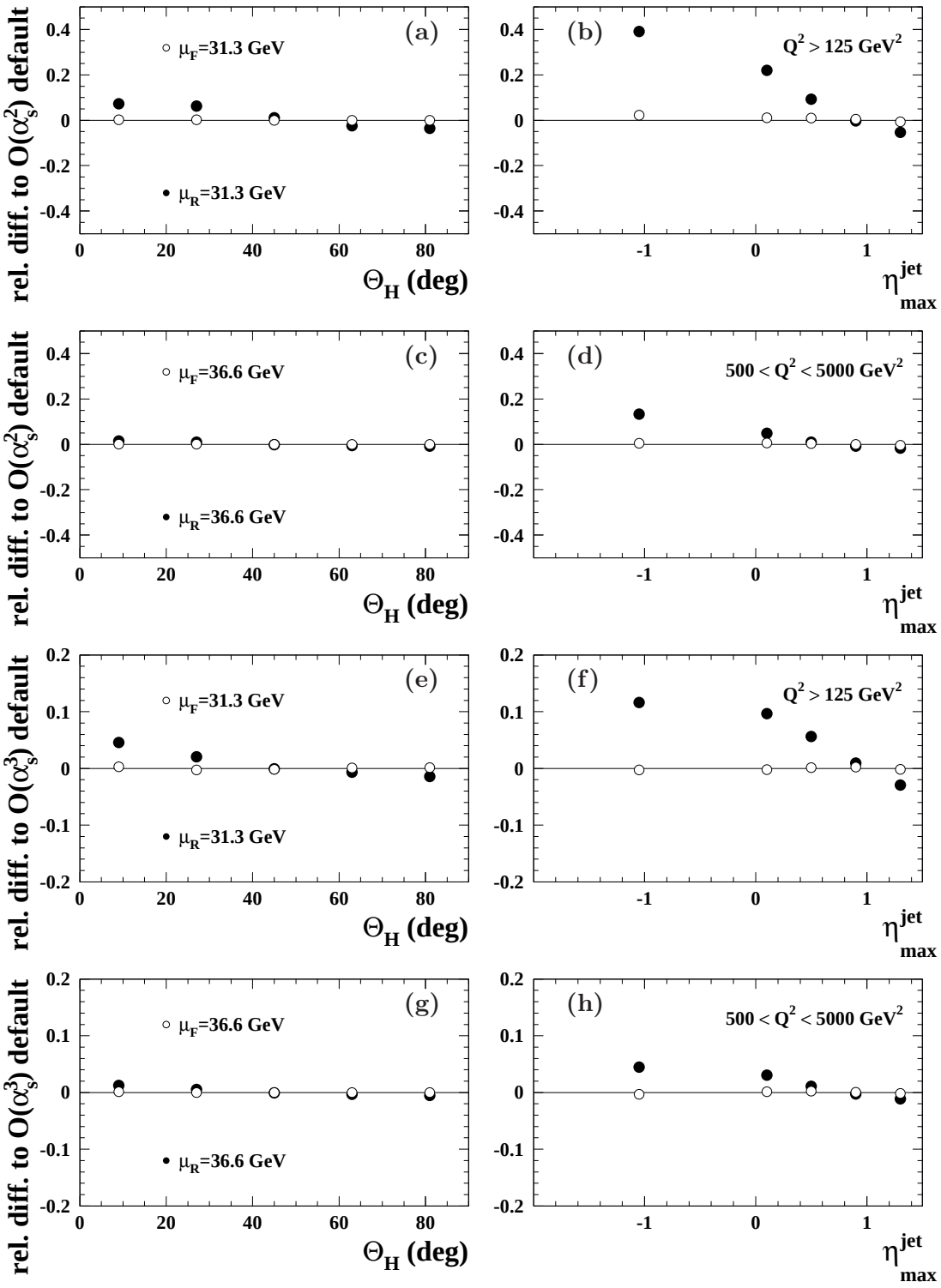

Figure 3: *Relative difference between the $\mathcal{O}(\alpha_s^2)$ normalised cross-section calculations with fixed μ_R and the calculations with $\mu_R = Q$ (dots) and between the $\mathcal{O}(\alpha_s^2)$ calculations with fixed μ_F and the calculations with $\mu_F = Q$ (open circles) in NC DIS for $Q^2 > 125$ GeV^2 as functions of (a) θ_H and (b) $\eta^{\rm jet}_{\rm max}$. (c) and (d) show the corresponding relative differences for $500 < Q^2 < 5000$ GeV^2. (e) to (h) show the corresponding relative differences using the $\mathcal{O}(\alpha_s^3)$ calculations. All these calculations do not include corrections for hadronisation effects.*

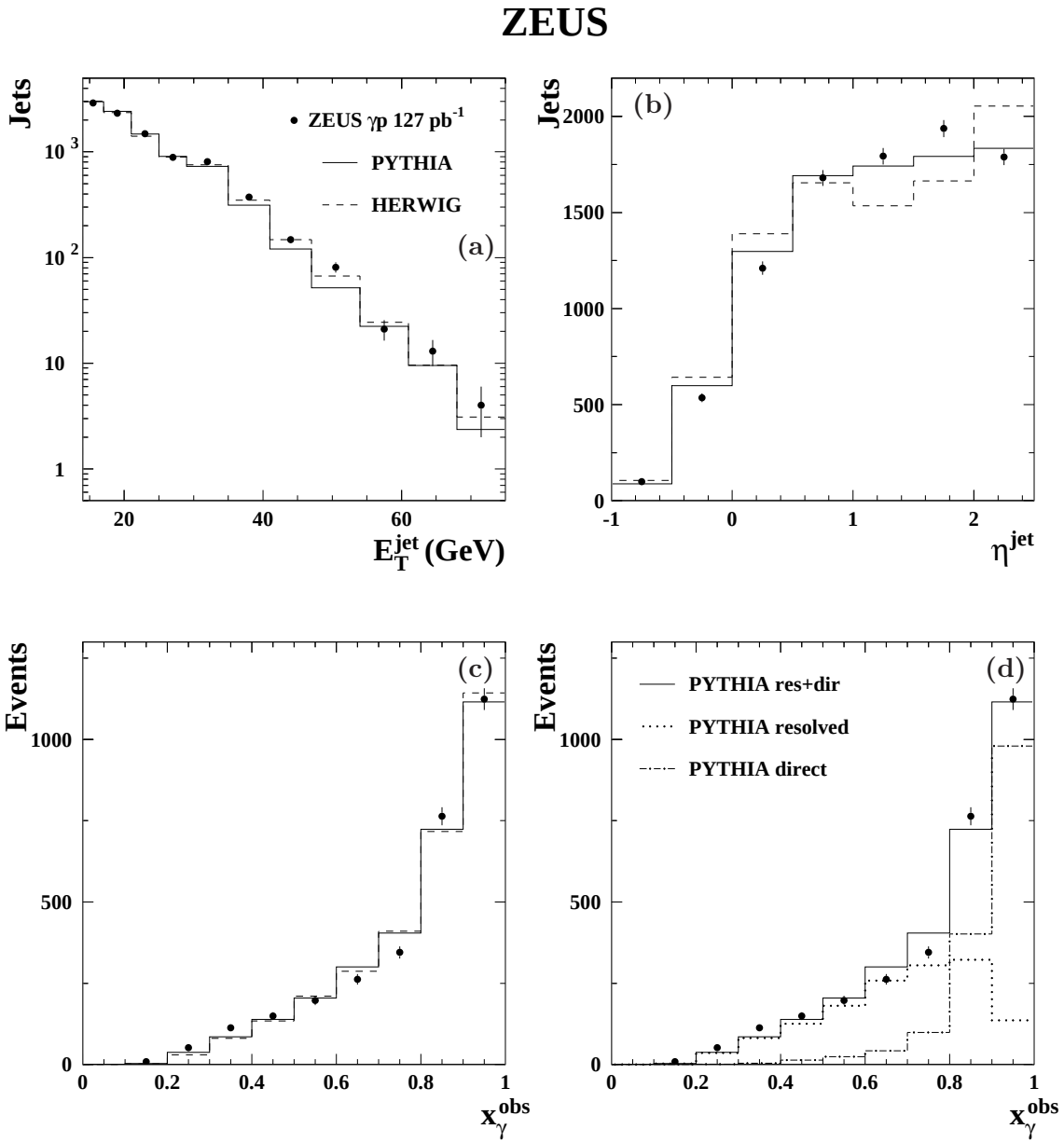

Figure 4: *Detector-level data distributions for three-jet photoproduction (dots) with* $E_T^{\rm jet} > 14$ *GeV and* $-1 < \eta^{\rm jet} < 2.5$ *in the kinematic region given by* $Q^2 < 1$ *GeV*^{2} *and* $0.2 < y < 0.85$ *as functions of (a)* $E_T^{\rm jet}$*, (b)* $\eta^{\rm jet}$ *and (c,d)* $x_\gamma^{\rm obs}$*. For comparison, the distributions of the* PYTHIA *(solid histograms) and* HERWIG *(dashed histograms) MC models for resolved plus direct processes normalised to the data are included. In (d), the contributions for resolved (dotted histogram) and direct (dot-dashed histogram) processes from* PYTHIA *MC are shown separately.*

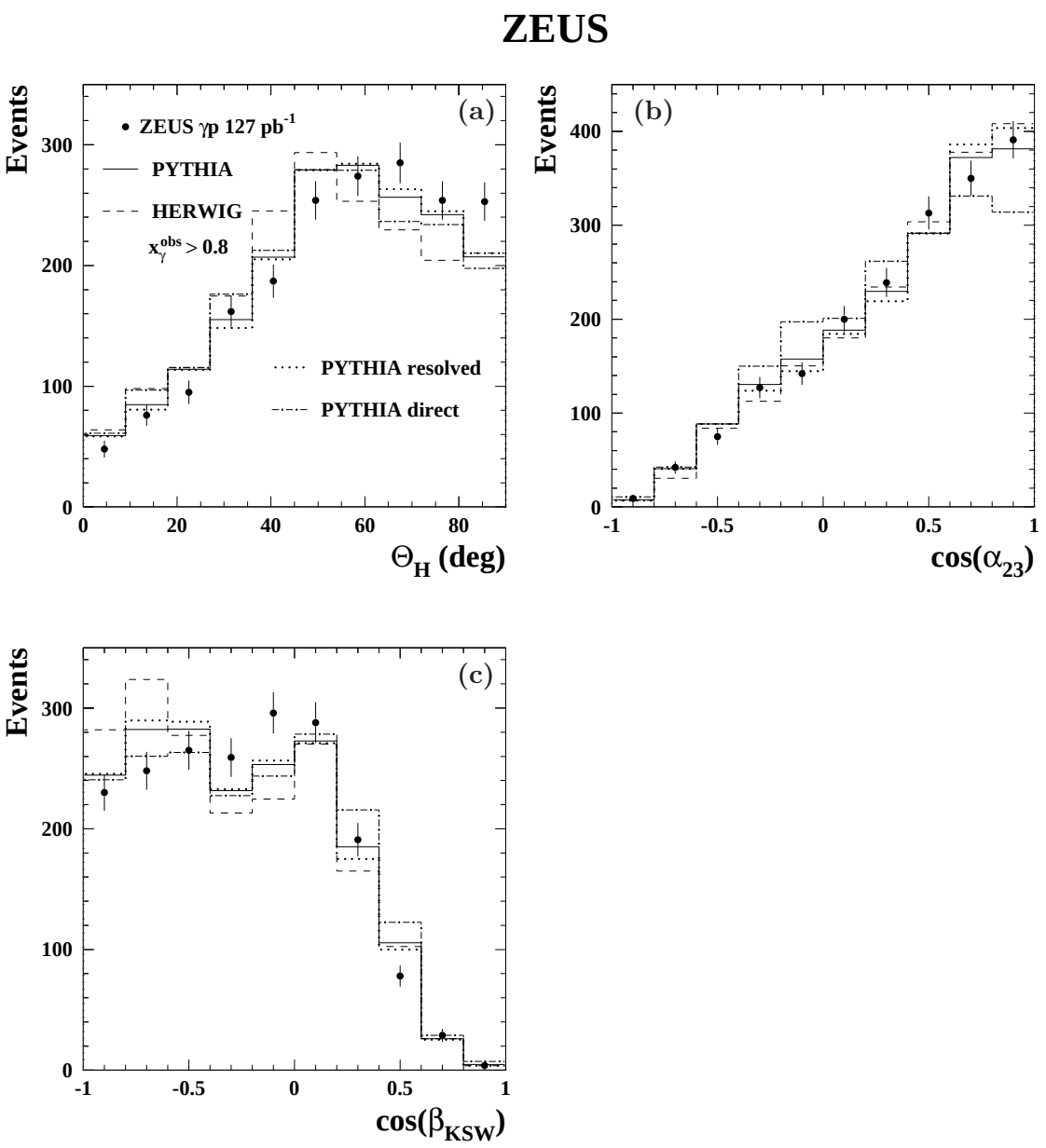

Figure 5: *Detector-level data distributions for three-jet photoproduction (dots) with* $E_T^{\rm jet} > 14$ *GeV and* $-1 < \eta^{\rm jet} < 2.5$ *in the kinematic region given by* $Q^2 < 1$ *GeV*^{2}, $0.2 < y < 0.85$ *and* $x_\gamma^{\rm obs} > 0.8$ *as functions of (a)* θ_H, *(b)* $\cos(\alpha_{23})$ *and (c)* $\cos(\beta_{\rm KSW})$. *Other details as in the caption to Fig. 4.*

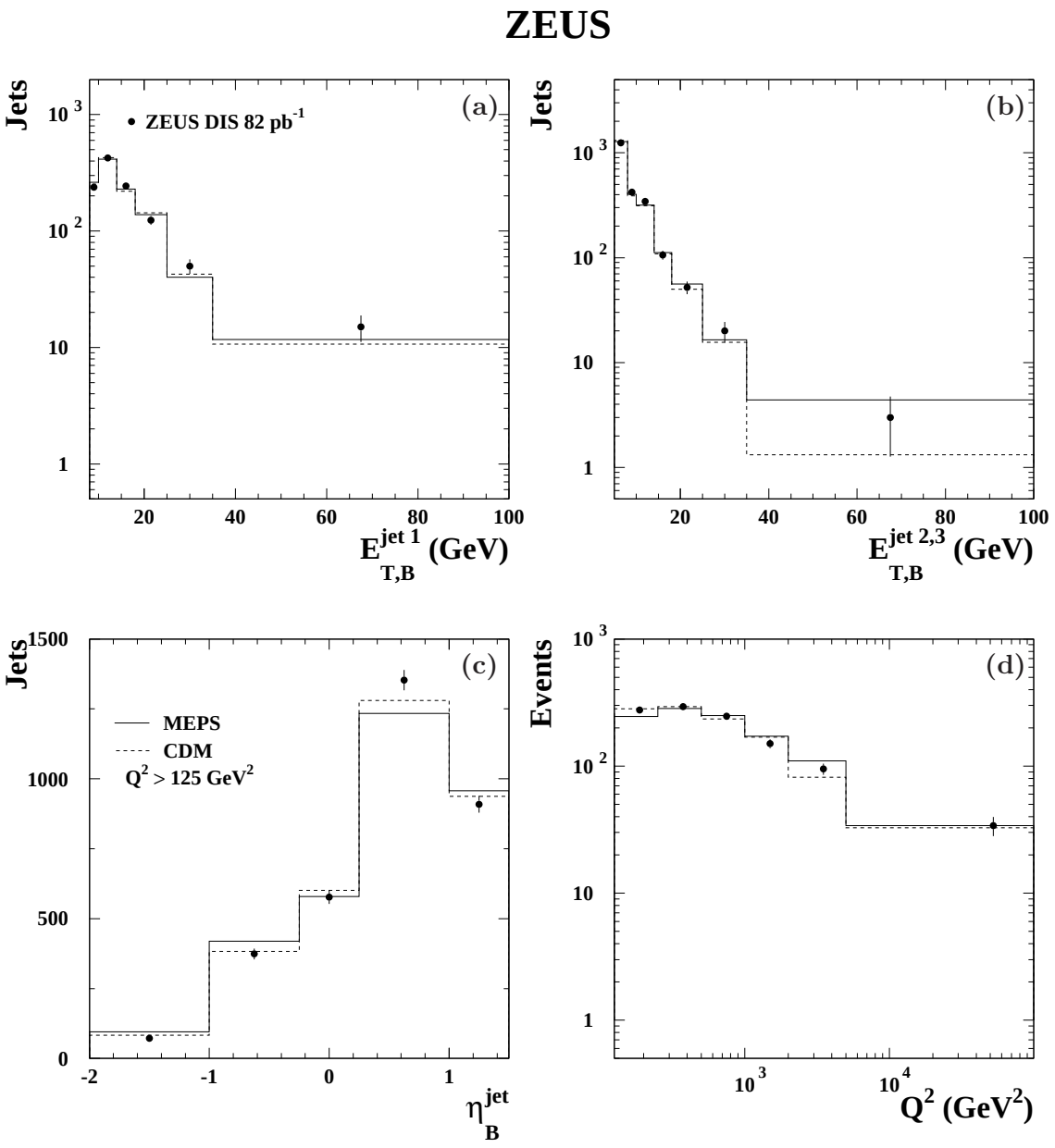

Figure 6: *Detector-level data distributions for three-jet production in NC DIS (dots) with* $E_{T,\mathrm{B}}^{\mathrm{jet1}} > 8$ *GeV,* $E_{T,\mathrm{B}}^{\mathrm{jet2,3}} > 5$ *GeV and* $-2 < \eta_{\mathrm{B}}^{\mathrm{jet}} < 1.5$ *in the kinematic region given by* $Q^2 > 125$ GeV^2 *and* $|\cos\gamma_h| < 0.65$ *as functions of (a)* $E_{T,\mathrm{B}}^{\mathrm{jet1}}$*, (b)* $E_{T,\mathrm{B}}^{\mathrm{jet2,3}}$*, (c)* $\eta_{\mathrm{B}}^{\mathrm{jet}}$ *and (d)* Q^2*. For comparison, the distributions of the MEPS (solid histograms) and CDM (dashed histograms) MC models normalised to the data are included.*

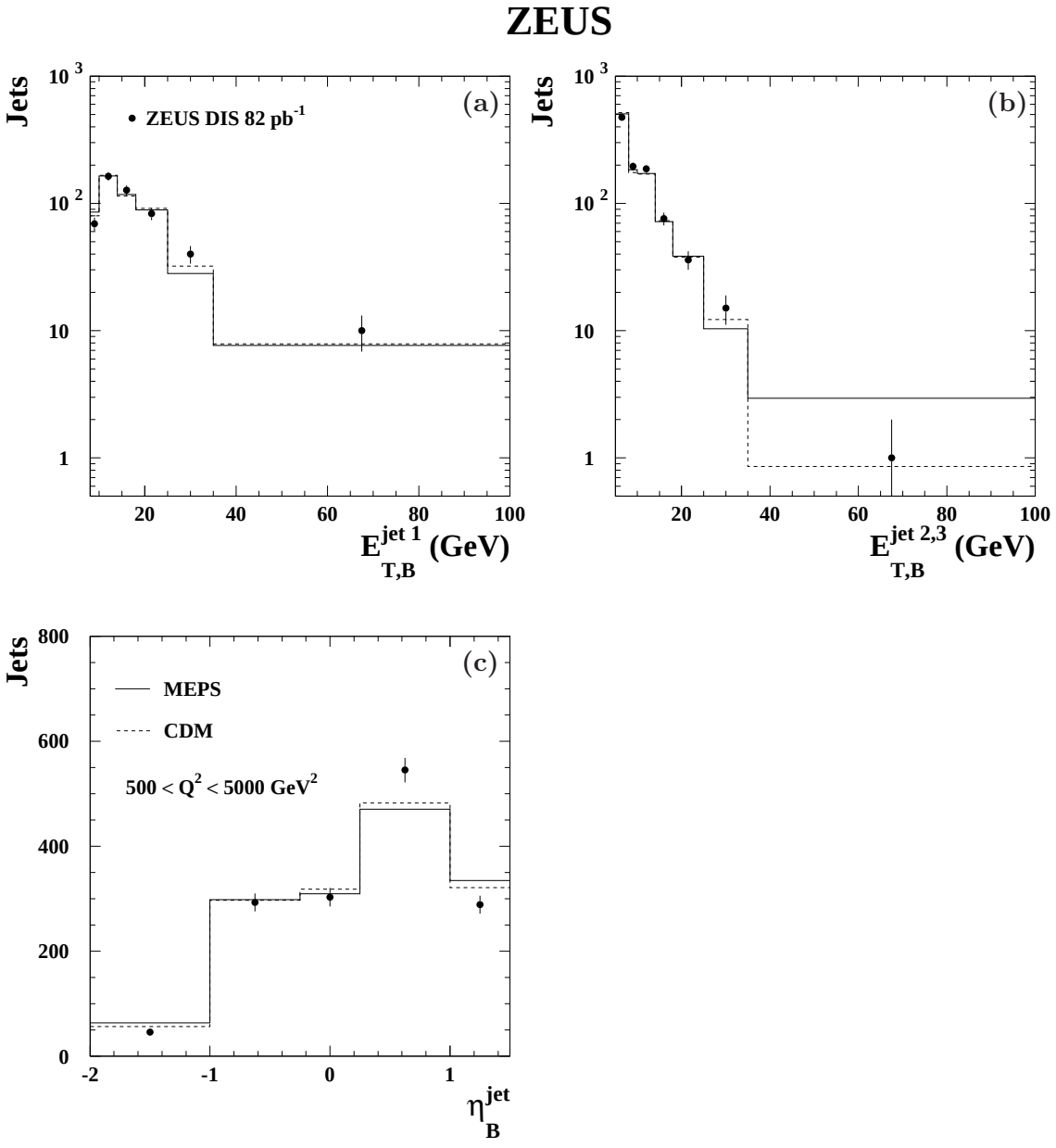

Figure 7: *Detector-level data distributions for three-jet production in NC DIS (dots) with* $E_{T,\mathrm{B}}^{\mathrm{jet1}} > 8$ *GeV,* $E_{T,\mathrm{B}}^{\mathrm{jet2,3}} > 5$ *GeV and* $-2 < \eta_{\mathrm{B}}^{\mathrm{jet}} < 1.5$ *in the kinematic region given by* $500 < Q^2 < 5000$ GeV^2 *and* $|\cos\gamma_h| < 0.65$ *as functions of (a)* $E_{T,\mathrm{B}}^{\mathrm{jet1}}$*, (b)* $E_{T,\mathrm{B}}^{\mathrm{jet2,3}}$ *and (c)* $\eta_{\mathrm{B}}^{\mathrm{jet}}$*. Other details as in the caption to Fig. 6.*

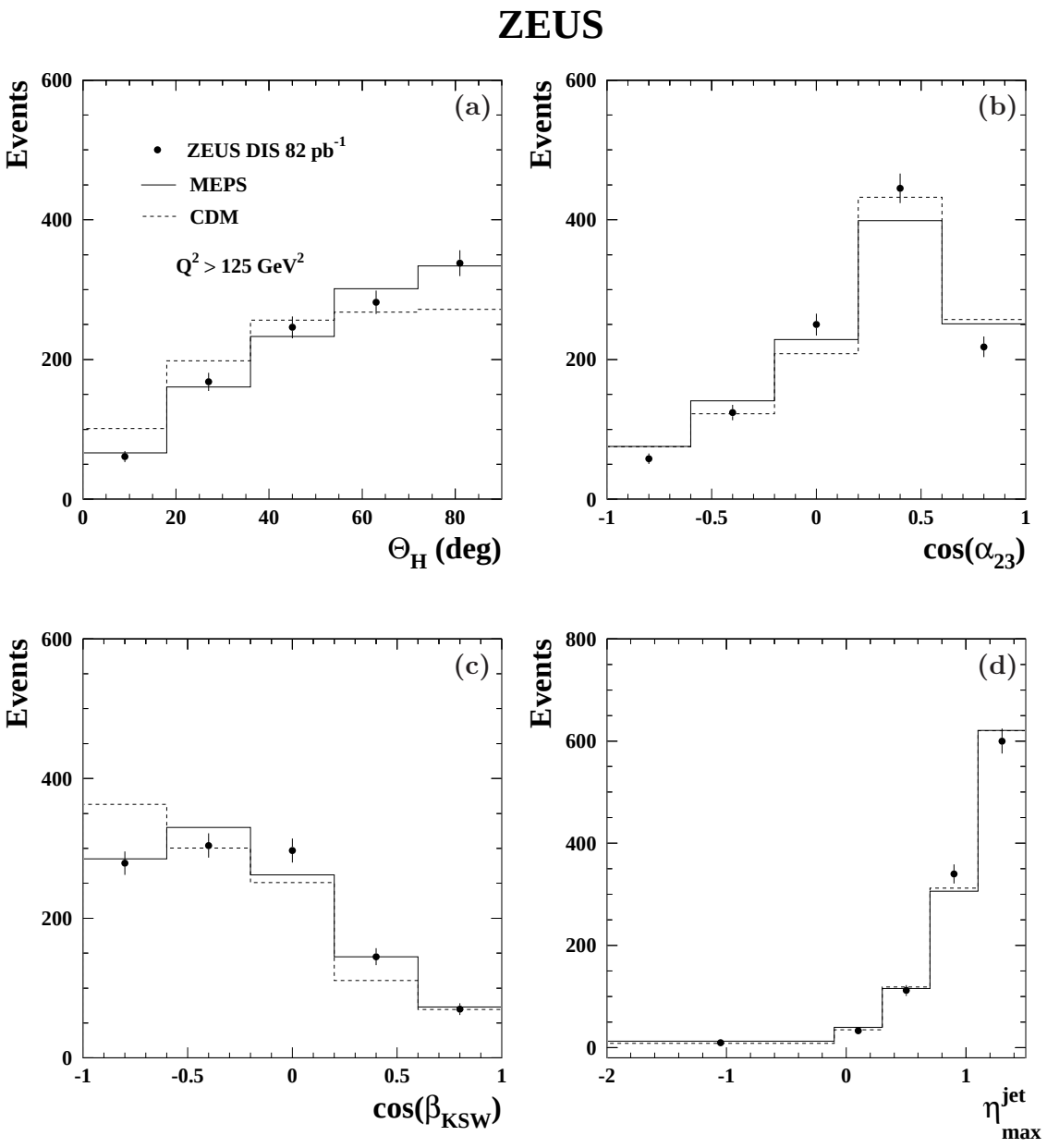

Figure 8: *Detector-level data distributions for three-jet production in NC DIS (dots) with* $E_{T,\mathrm{B}}^{\mathrm{jet1}} > 8$ *GeV,* $E_{T,\mathrm{B}}^{\mathrm{jet2,3}} > 5$ *GeV and* $-2 < \eta_{\mathrm{B}}^{\mathrm{jet}} < 1.5$ *in the kinematic region given by* $Q^2 > 125$ GeV^2 *and* $|\cos\gamma_h| < 0.65$ *as functions of (a)* θ_H*, (b)* $\cos(\alpha_{23})$*, (c)* $\cos(\beta_{\mathrm{KSW}})$ *and (d)* $\eta_{\mathrm{max}}^{\mathrm{jet}}$*. For comparison, the distributions of the MEPS (solid histograms) and CDM (dashed histograms) MC models normalised to the data are included.*

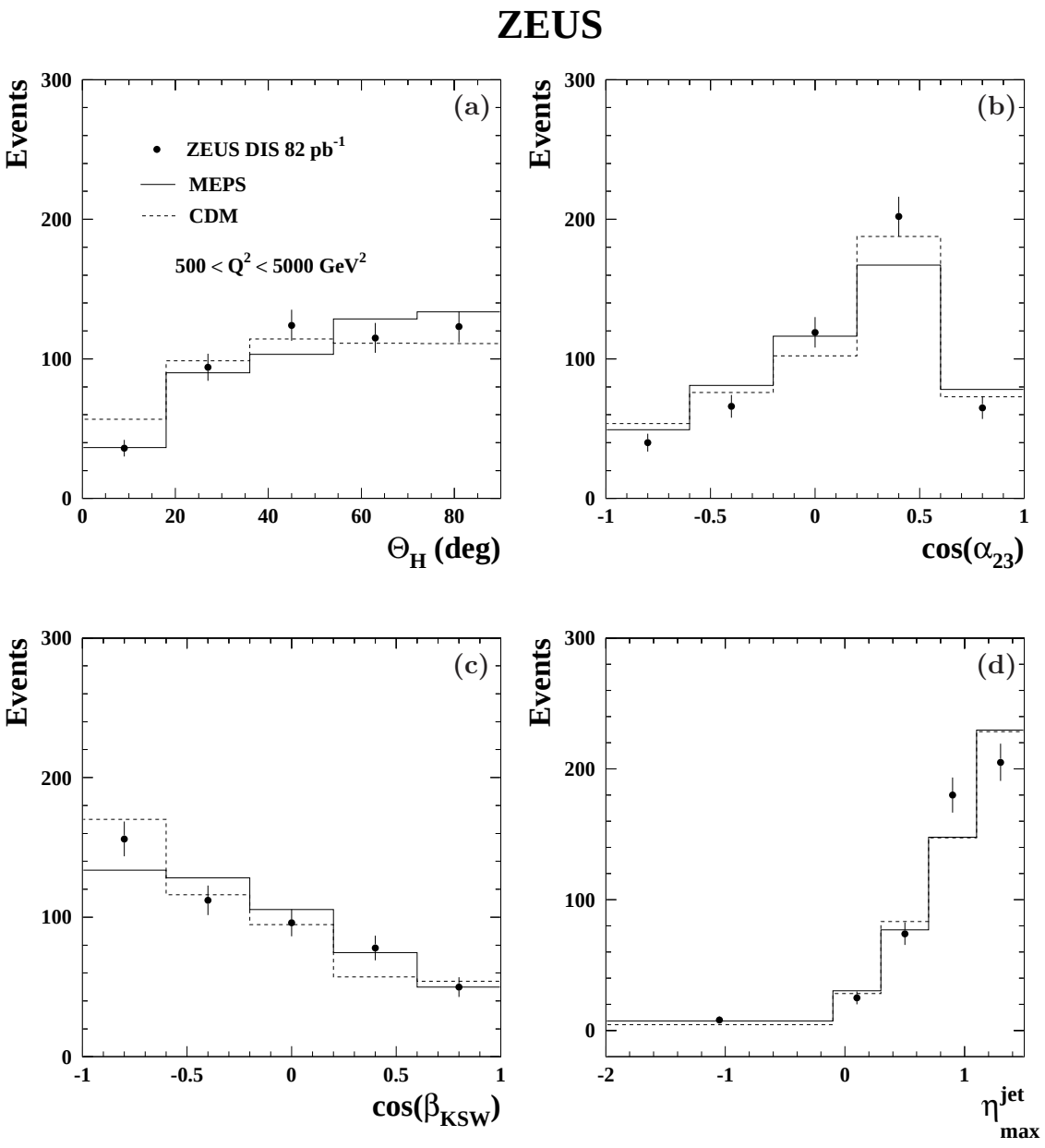

Figure 9: *Detector-level data distributions for three-jet production in NC DIS (dots) with* $E_{T,\mathrm{B}}^{\mathrm{jet1}} > 8$ *GeV,* $E_{T,\mathrm{B}}^{\mathrm{jet2,3}} > 5$ *GeV and* $-2 < \eta_{\mathrm{B}}^{\mathrm{jet}} < 1.5$ *in the kinematic region given by* $500 < Q^2 < 5000$ GeV^2 *and* $|\cos\gamma_h| < 0.65$ *as functions of (a)* θ_H*, (b)* $\cos(\alpha_{23})$*, (c)* $\cos(\beta_{\mathrm{KSW}})$ *and (d)* $\eta_{\mathrm{max}}^{\mathrm{jet}}$*. Other details as in the caption to Fig. 8.*

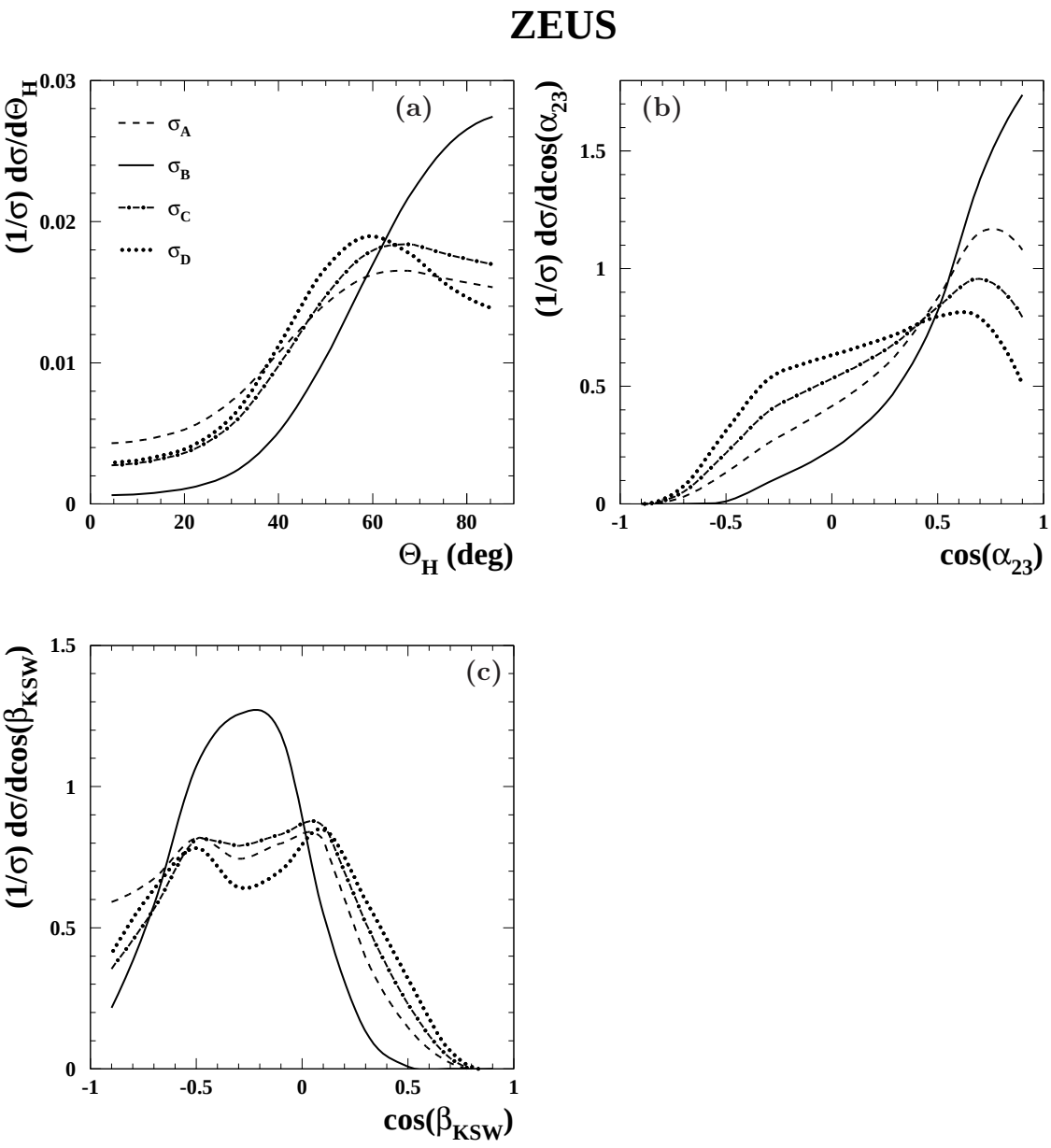

Figure 10: *Predicted normalised differential ep cross sections for three-jet direct-photon processes at $\mathcal{O}(\alpha_s^2)$ integrated over $E_T^{\rm jet} > 14$ GeV and $-1 < \eta^{\rm jet} < 2.5$ in the kinematic region defined by $Q^2 < 1$ GeV^2 and $0.2 < y < 0.85$ as functions of (a) θ_H, (b) $\cos(\alpha_{23})$ and (c) $\cos(\beta_{\rm KSW})$. In each figure, the predictions for the colour components are shown: σ_A (dashed lines), σ_B (solid lines), σ_C (dot-dashed lines) and σ_D (dotted lines). These calculations do not include corrections for hadronisation effects.*

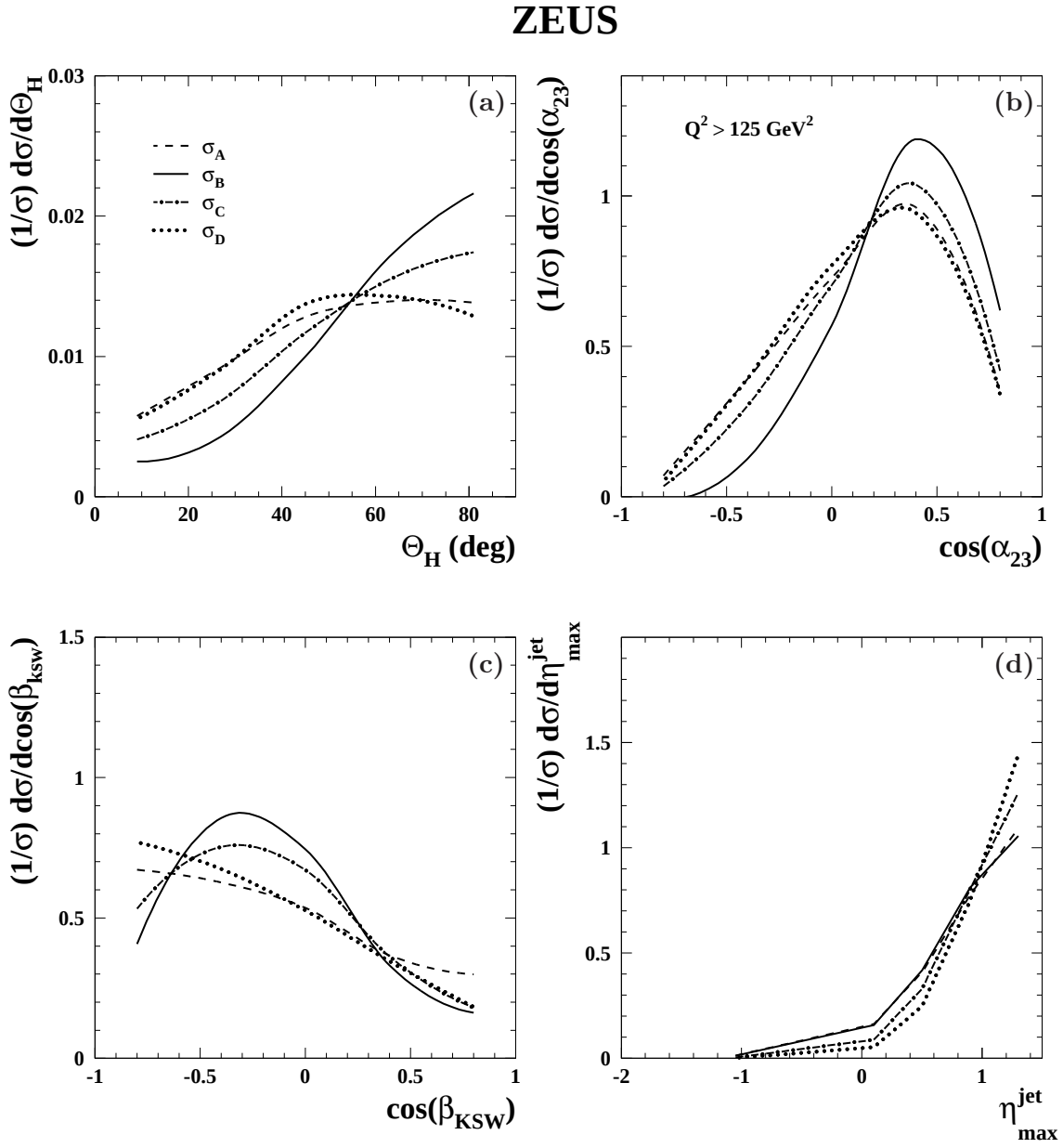

Figure 11: *Predicted normalised differential ep cross sections for three-jet production in NC DIS at $\mathcal{O}(\alpha_s^2)$ integrated over $E_{T,\mathrm{B}}^{\mathrm{jet1}} > 8$ GeV, $E_{T,\mathrm{B}}^{\mathrm{jet2,3}} > 5$ GeV and $-2 < \eta_{\mathrm{B}}^{\mathrm{jet}} < 1.5$ in the kinematic region given by $Q^2 > 125$ GeV^2 and $|\cos\gamma_h| < 0.65$ as functions of (a) θ_H, (b) $\cos(\alpha_{23})$, (c) $\cos(\beta_{\mathrm{KSW}})$ and (d) $\eta_{\mathrm{max}}^{\mathrm{jet}}$. Other details as in the caption to Fig. 10. These calculations do not include corrections for hadronisation effects.*

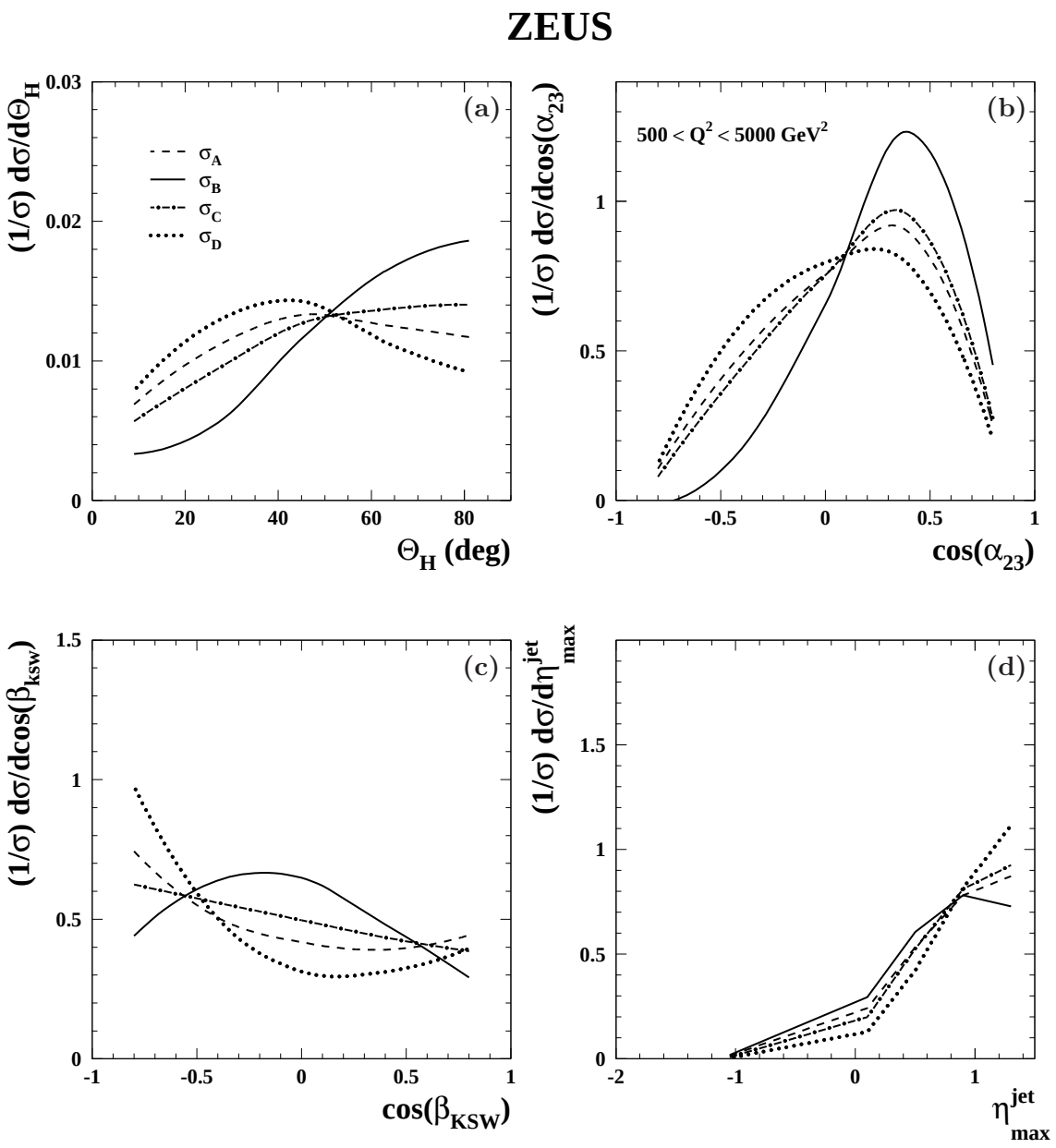

Figure 12: *Predicted normalised differential ep cross sections for three-jet production in NC DIS at $\mathcal{O}(\alpha_s^2)$ integrated over $E_{T,\mathrm{B}}^{\mathrm{jet1}} > 8$ GeV, $E_{T,\mathrm{B}}^{\mathrm{jet2,3}} > 5$ GeV and $-2 < \eta_{\mathrm{B}}^{\mathrm{jet}} < 1.5$ in the kinematic region given by $500 < Q^2 < 5000$ GeV^2 and $|\cos\gamma_h| < 0.65$ as functions of (a) θ_H, (b) $\cos(\alpha_{23})$, (c) $\cos(\beta_{\mathrm{KSW}})$ and (d) $\eta_{\mathrm{max}}^{\mathrm{jet}}$. Other details as in the caption to Fig. 10. These calculations do not include corrections for hadronisation effects.*

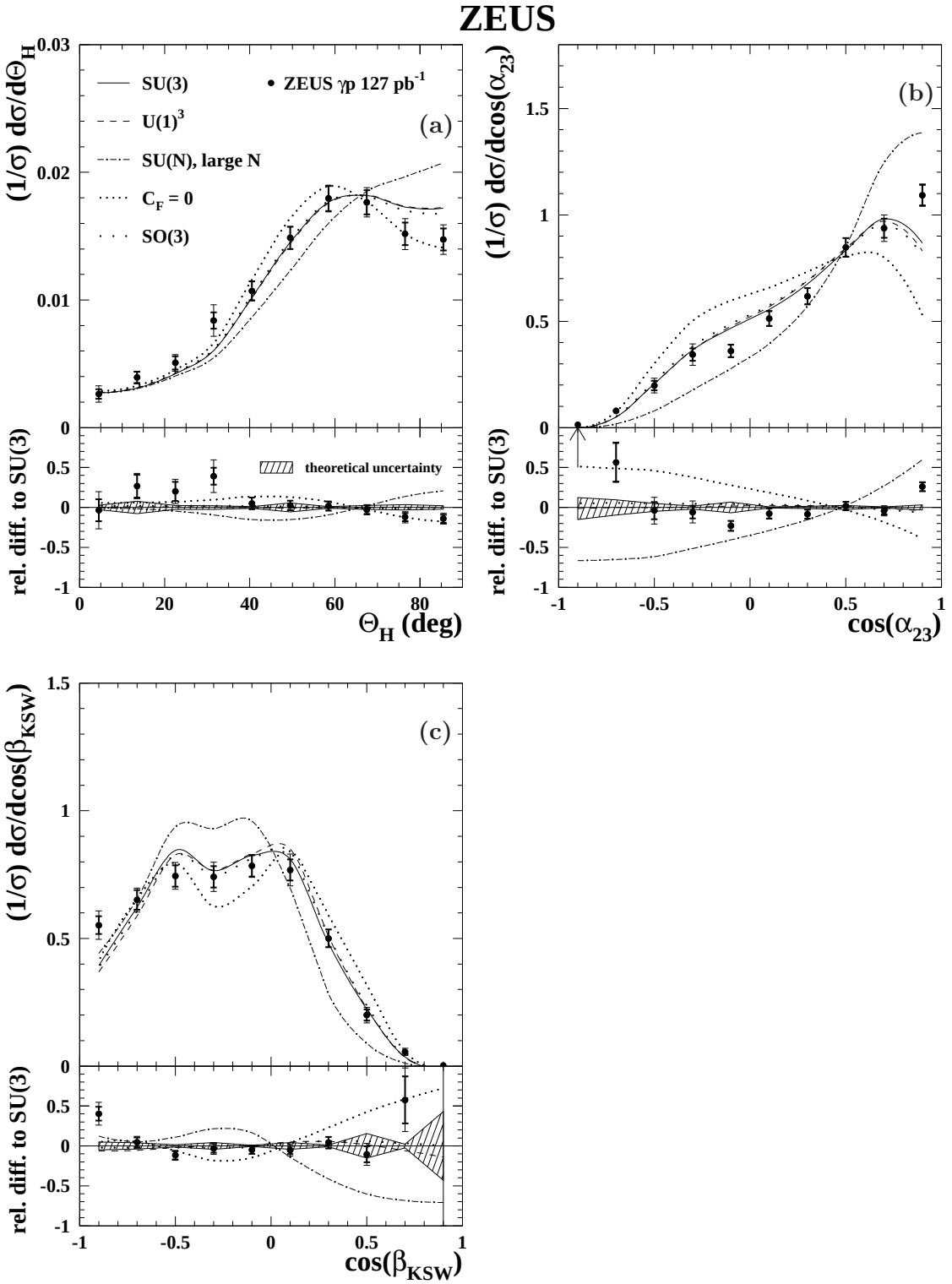

Figure 13: *Measured normalised differential ep cross sections for three-jet photoproduction (dots) integrated over $E_T^{\rm jet} > 14$ GeV and $-1 < \eta^{\rm jet} < 2.5$ in the kinematic region defined by $Q^2 < 1$ GeV^2, $0.2 < y < 0.85$ and $x_\gamma^{\rm obs} > 0.8$ as functions of (a) θ_H, (b) $\cos(\alpha_{23})$ and (c) $\cos(\beta_{\rm KSW})$. The data points are plotted at the bin centres. The inner error bars represent the statistical uncertainties of the data, and the outer error bars show the statistical and systematic uncertainties added in quadrature. For comparison, the $\mathcal{O}(\alpha_s^2)$ calculations for direct-photon processes based on SU(3) (solid lines), U(1)^3 (dashed lines), SU(N) in the limit of large N (dot-dashed lines), $C_F = 0$ (short-spaced dotted lines) and SO(3) (long-spaced dotted lines) are included. The lower part of the figures displays the relative difference to the calculations based on SU(3) and the hatched band shows the relative uncertainty of this calculation.*

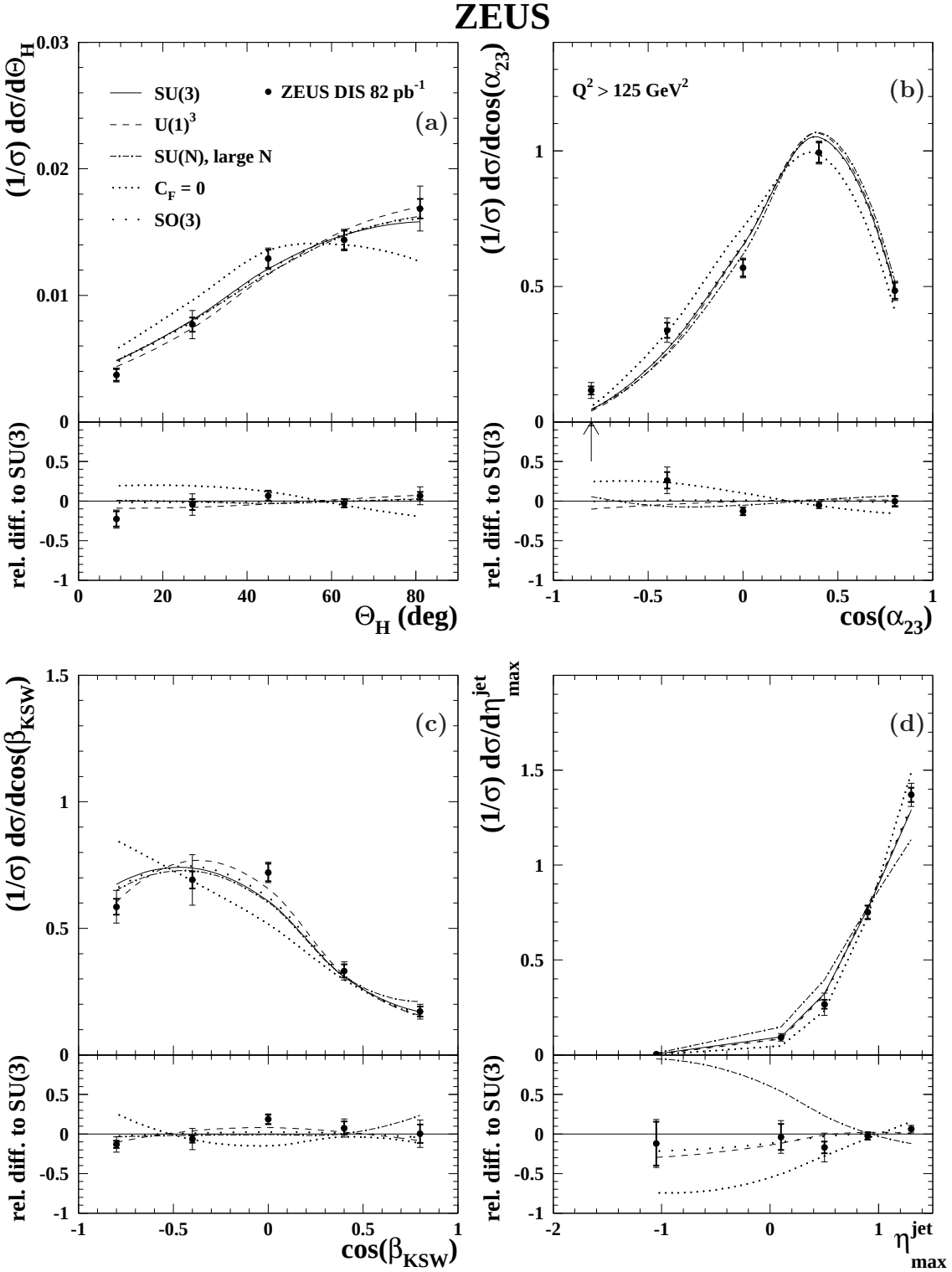

Figure 14: *Measured normalised differential ep cross sections for three-jet production in NC DIS (dots) integrated over* $E_{T,\mathrm{B}}^{\mathrm{jet1}} > 8$ *GeV,* $E_{T,\mathrm{B}}^{\mathrm{jet2,3}} > 5$ *GeV and* $-2 < \eta_{\mathrm{B}}^{\mathrm{jet}} < 1.5$ *in the kinematic region given by* $Q^2 > 125$ GeV^2 *and* $|\cos\gamma_h| < 0.65$ *as functions of (a)* θ_H*, (b)* $\cos(\alpha_{23})$*, (c)* $\cos(\beta_{\mathrm{KSW}})$ *and (d)* $\eta_{\mathrm{max}}^{\mathrm{jet}}$*. Other details as in the caption to Fig. 13.*

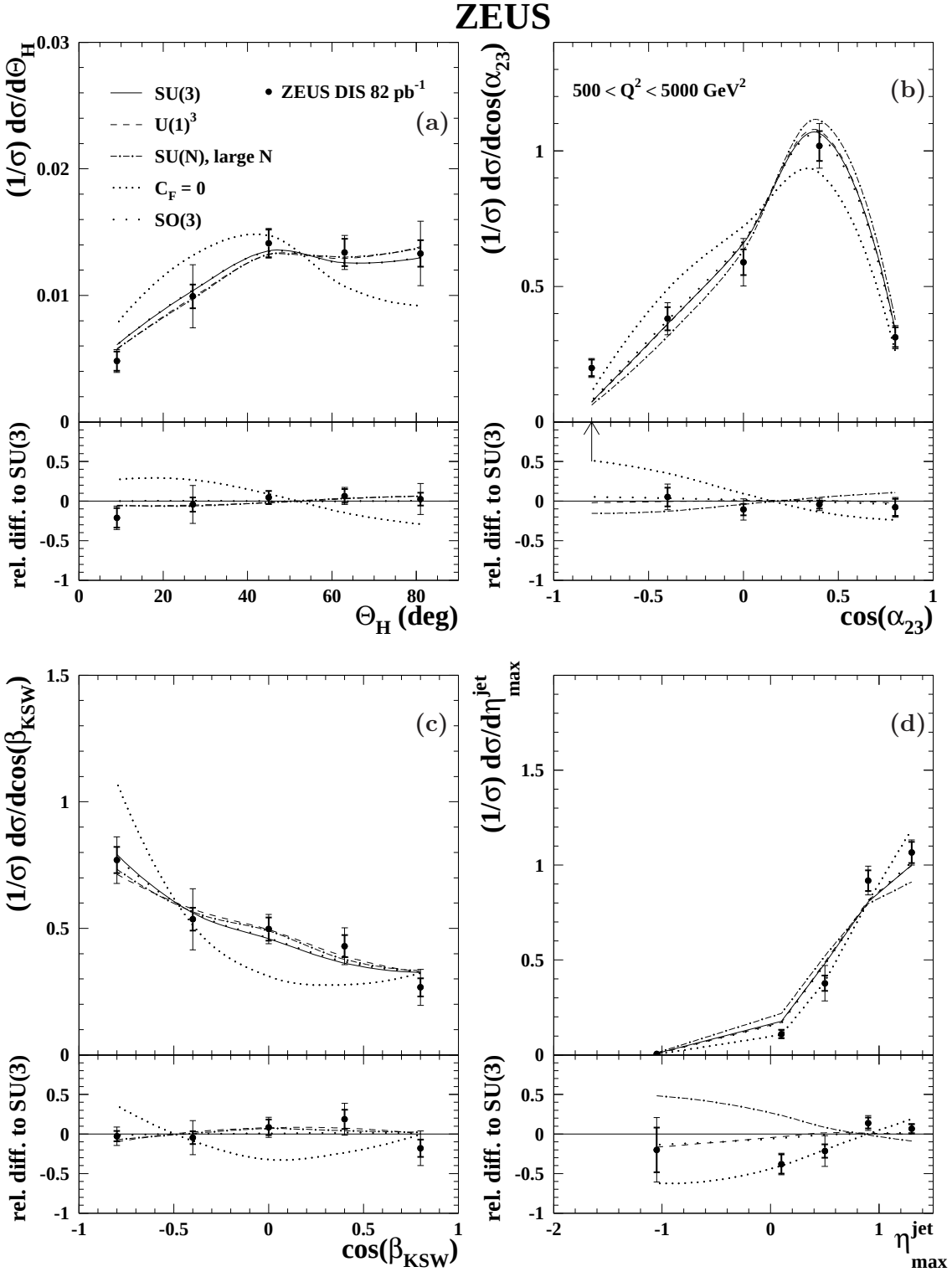

Figure 15: *Measured normalised differential ep cross sections for three-jet production in NC DIS (dots) integrated over* $E_{T,\mathrm{B}}^{\mathrm{jet1}} > 8$ *GeV,* $E_{T,\mathrm{B}}^{\mathrm{jet2,3}} > 5$ *GeV and* $-2 < \eta_{\mathrm{B}}^{\mathrm{jet}} < 1.5$ *in the kinematic region given by* $500 < Q^2 < 5000$ GeV^2 *and* $|\cos\gamma_h| < 0.65$ *as functions of (a)* θ_H*, (b)* $\cos(\alpha_{23})$*, (c)* $\cos(\beta_{\mathrm{KSW}})$ *and (d)* $\eta_{\mathrm{max}}^{\mathrm{jet}}$*. Other details as in the caption to Fig. 13.*

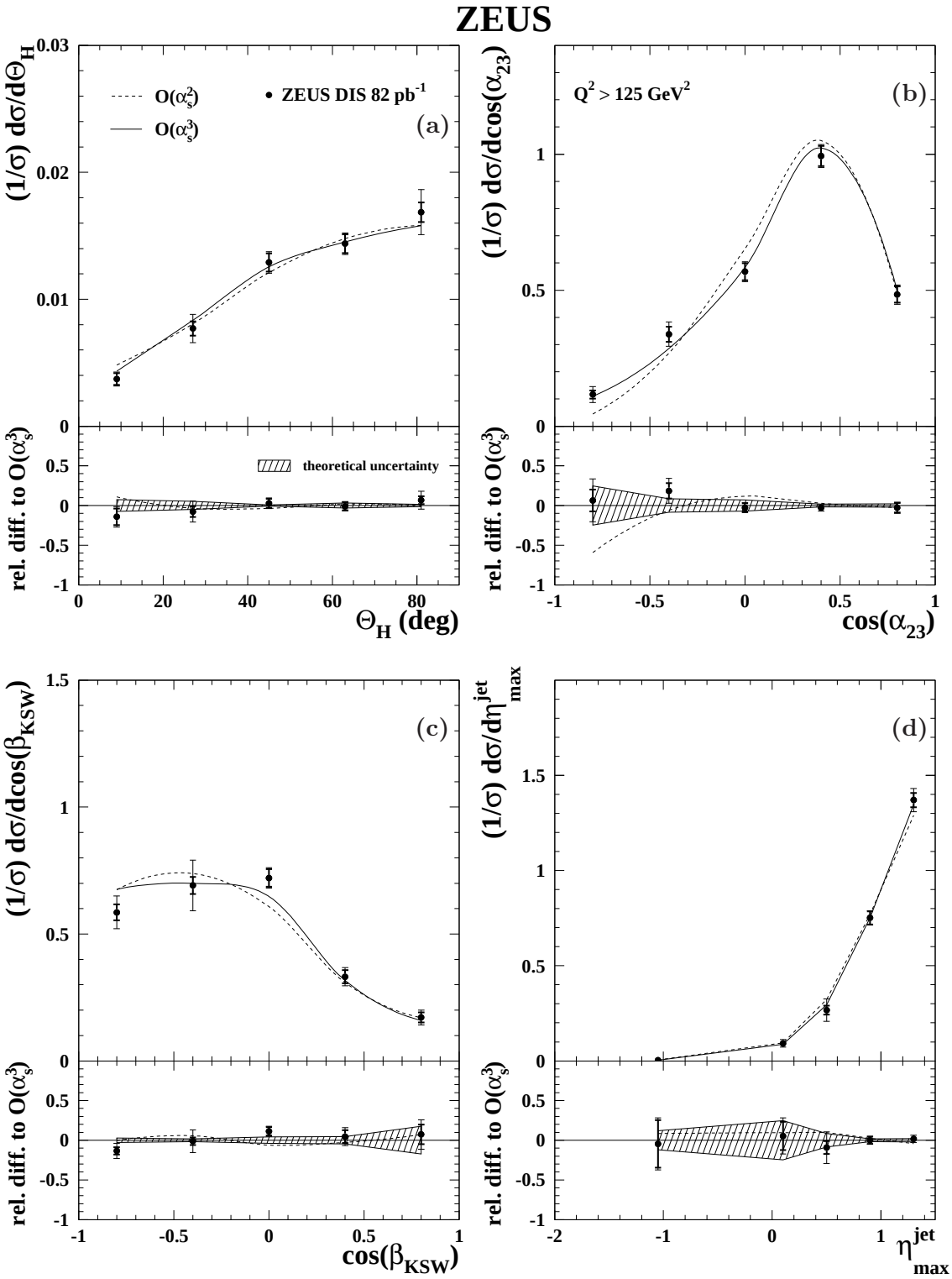

Figure 16: *Measured normalised differential ep cross sections for three-jet production in NC DIS (dots) integrated over* $E_{T,\mathrm{B}}^{\mathrm{jet1}} > 8$ *GeV,* $E_{T,\mathrm{B}}^{\mathrm{jet2,3}} > 5$ *GeV and* $-2 < \eta_{\mathrm{B}}^{\mathrm{jet}} < 1.5$ *in the kinematic region given by* $Q^2 > 125$ GeV^2 *and* $|\cos\gamma_h| < 0.65$ *as functions of (a)* θ_H*, (b)* $\cos(\alpha_{23})$*, (c)* $\cos(\beta_{\mathrm{KSW}})$ *and (d)* $\eta_{\mathrm{max}}^{\mathrm{jet}}$*. For comparison, the* $\mathcal{O}(\alpha_s^2)$ *(dashed lines) and* $\mathcal{O}(\alpha_s^3)$ *(solid lines) QCD calculations are also included. The hatched band displays the relative theoretical uncertainty of the* $\mathcal{O}(\alpha_s^3)$ *calculation. Other details as in the caption to Fig. 13.*

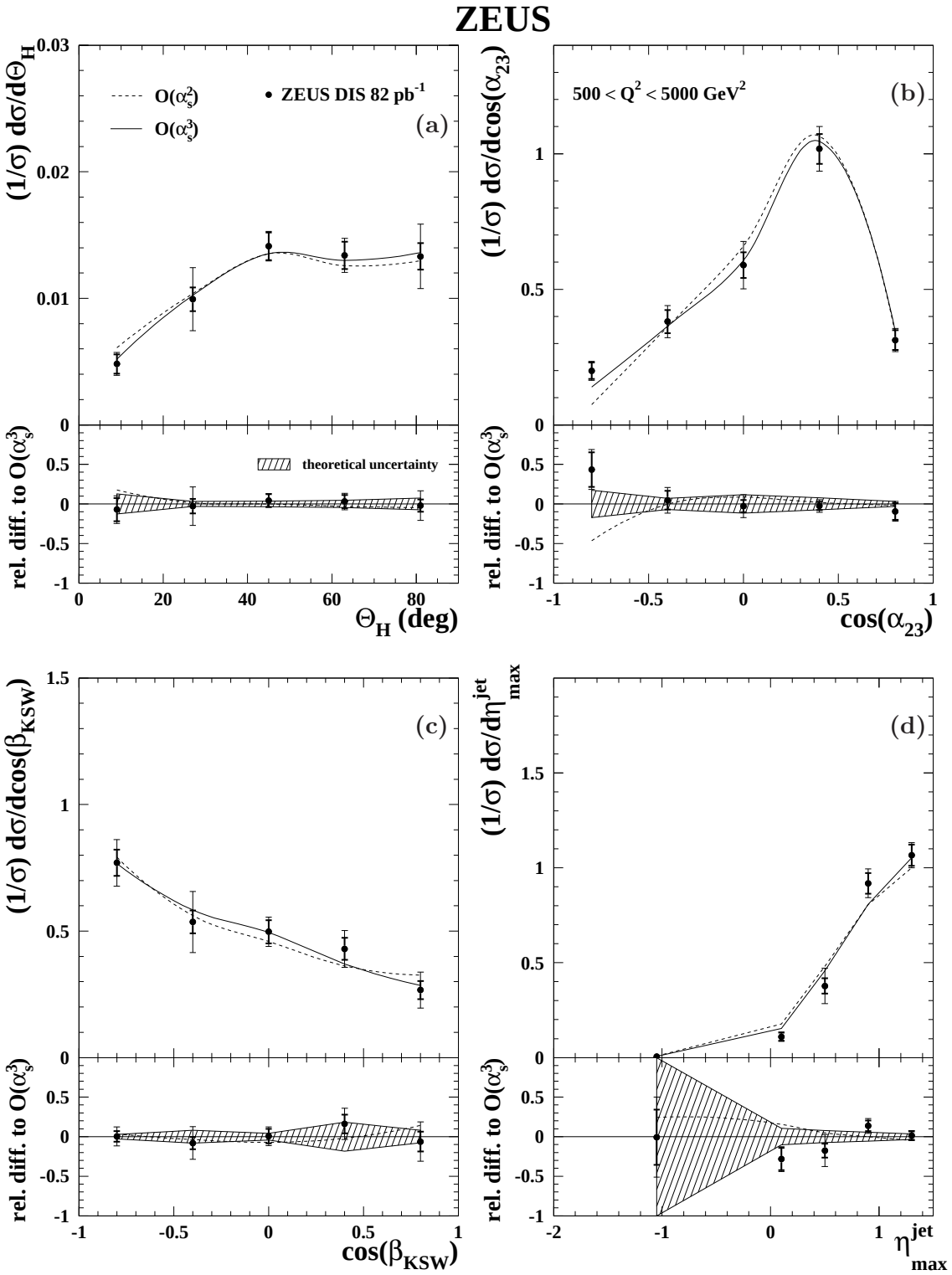

Figure 17: *Measured normalised differential ep cross sections for three-jet production in NC DIS (dots) integrated over* $E_{T,\mathrm{B}}^{\mathrm{jet1}} > 8$ *GeV,* $E_{T,\mathrm{B}}^{\mathrm{jet2,3}} > 5$ *GeV and* $-2 < \eta_{\mathrm{B}}^{\mathrm{jet}} < 1.5$ *in the kinematic region given by* $500 < Q^2 < 5000$ GeV^2 *and* $|\cos\gamma_h| < 0.65$ *as functions of (a)* θ_H*, (b)* $\cos(\alpha_{23})$*, (c)* $\cos(\beta_{\mathrm{KSW}})$ *and (d)* $\eta_{\mathrm{max}}^{\mathrm{jet}}$*. For comparison, the* $\mathcal{O}(\alpha_s^2)$ *(dashed lines) and* $\mathcal{O}(\alpha_s^3)$ *(solid lines) QCD calculations are also included. The hatched band displays the relative theoretical uncertainty of the* $\mathcal{O}(\alpha_s^3)$ *calculation. Other details as in the caption to Fig. 13.*